Iron and aluminum association with microbially processed organic matter via meso-density aggregate formation across soils: organo-metallic glue hypothesis

5   Rota Wagai[1], Masako Kajiura[1], Maki Asano[2]

[1]National Agriculture and Food Research Organization, Institute for Agro-Environmental Sciences. 3-1-3 Kan-nondai, Tsukuba, Ibaraki, 305-8604, Japan
[2]Faculty of Life and Environmental Sciences, University of Tsukuba, 1-1-1 Tennodai, Tsukuba, Ibaraki 305-8572, Japan

Correspondence to: Rota Wagai (rota@affrc.go.jp)

10   **Abstract.** Global significance of iron (Fe) and aluminum (Al) for the storage of organic matter (OM) in soils and surface sediments is increasingly recognized. Yet specific metal phases involved or the mechanism behind metal-OM correlations frequently shown across soils remain unclear. We identified the allocation of major metal phases and OM to density fractions using 23 soil samples from 5 climate zones and 5 soil orders (Andisols, Spodosols, Inceptisols, Mollisols, Ultisols) from Asia and North America, including several subsurface horizons and both natural and managed soils. Each soil was separated to 4 to 7 density fractions using sodium polytungstate with mechanical shaking, followed by the sequential extraction of each fraction with pyrophosphate (PP), acid oxalate (OX), and finally with dithionite-citrate (DC) to estimate pedogenic metal phases of different solubility and crystallinity. The concentrations of Fe and Al (per fraction) extracted by each of the three reagents were generally higher in meso-density fractions (1.8-2.4 g cm^{-3}) than in the lower- or higher-density fractions, showing a unique unimodal pattern along the particle density gradient for each soil. Across the studied soils, the maximum metal concentrations were always at the meso-density range within which PP-extractable metals peaked at 0.3-0.4 g cm^{-3} lower density range relative to OX- and DC-extractable metals. Meso-density fractions, consisting largely of aggregated clusters based on SEM observation, accounted for on average 56-70% of total extractable metals and OM present in these soils. The OM in meso-density fractions showed 2-23 unit lower C:N ratio than the lowest-density fraction of respective soil and thus appeared microbially processed relative to the original plant material. The amounts of PP- and OX-extractable metals correlated positively with co-dissolved C across the soils and, to some extent, across the density fractions within each soil. These results led to a hypothesis which involves two distinct levels of organo-metal interaction: (1) the formation of OM-rich, mixed metal phases with fixed OM:metal stoichiometry followed by (2) the development of meso-density microaggregates via "gluing" action of these organo-metallic phases by entraining other organic and mineral particles such as phyllosilicate clays. Given that OM is mainly located in meso-density fractions, a soil's capacity to protect OM may be controlled by the balance of three processes: (i) microbial processing of plant-derived OM, (ii) dissolution of metals, and (iii) the synthesis of organo-metallic phases and their association with clays to form meso-density microaggregates. The current hypothesis may help to fill

the gap between well-studied molecular scales interaction (e.g., OM adsorption on mineral surface, coprecipitation) and larger-scale processes such as aggregation, C accrual, and pedogenesis.

35 **1 Introduction**

Organic matter (OM) stored in soil plays a fundamental role in ecosystem functioning through the storage of carbon (C) and nutrients, improvement of aeration and water-holding capacity, and thus plant productivity and biogeochemical cycling. Changes in soil OM have a significant impact on future climate as soil represents the largest terrestrial C pool. The storage capacity and stability of soil OM are particularly important questions for our efforts to limit global warming (Smith, 2016).

40 Soil OM stability is strongly controlled by its association with soil minerals via chemical interaction and physical aggregation (Lehmann and Kleber, 2015; Sollins et al., 1996). The mineral parameters often used to estimate soil's protective capacity are clay content (<2 μm) or clay plus silt content (<20 μm) of soils as they often correlate with soil OM contents and these small-sized minerals tend to have high surface area to adsorb OM (Six et al., 2002 and the references therein). Commonly used mathematical models to predict soil C changes use these parameters to slow down OM turnover and to increase its storage

45 (Coleman and Jenkinson, 1996; Parton et al., 1987; Wieder et al., 2015).

On the other hand, the global significance of iron (Fe) and aluminum (Al) phases for OM storage in soil and surface sediments has been increasingly recognized. Using 5500 pedons around the world, Rasmussen et al. (2018) showed stronger control of organic C storage in non-arid soils by oxalate extractable metal content than by clay content. Important linkage among climate (esp. water balance), dissolved organic C production, and its stabilization by these metal phases has been shown

50 on a continental scale (Kramer and Chadwick, 2018). Surface marine sediments also store significant amounts of Fe-bound C (Lalonde et al., 2012). Iron and aluminum, the third and fourth most abundant elements on the earth crust, are in fact highly reactive with OM once released via chemical weathering. These pedogenic Fe and Al can be present in monomeric form by chelating with organic ligands or in polymeric form as polynuclear complexes and as secondary minerals. The latter includes Fe and Al oxides, hydroxides, and oxyhydroxides (collectively called metal oxides, hereafter) as well as short-range-order

55 aluminosilicates (allophane, imogolite, and proto-imogolite) that have high sorptive capacity for OM due to their small size (down to several nm) and high surface reactivity via surface hydroxyl groups (Fuji et al., 2019; Kaiser and Guggenberger, 2003; Kleber et al., 2015). In addition, soluble complexes of Fe and Al with organic ligands can be precipitated especially in acidic, OM-rich environments such as volcanic and podzolic soils (Lundström et al., 2000; Percival et al., 2000; Takahashi and Dahlgren, 2016).

60 Incorporating such metal control into soil C models is still a challenge because the mechanisms by which pedogenic metals control OM storage and stabilization remain elusive. This is partly because current understanding relies largely on OM-metal correlations where the metal concentration often co-varies with other soil properties. The reactive metal contents often positively correlate with other mineralogical parameters that are considered to contribute to OM storage such as clay content

and soil specific surface area (e.g., Kaiser and Guggenberger, 2003; Mayer and Xing, 2001). In long-term pedogenesis (240-4,100 kys) under temperate or tropical moist climate regime, radiocarbon-based soil C age was positively correlated with extractable metal contents in two chronosequence studies (Masiello et al., 2004; Torn et al., 1997) but not in another study under wetter climate where only soil specific surface area and halloysite content showed significant correlation (Lawrence et al., 2015). Short-range-order minerals and Fe oxides can also promote aggregation (Churchman and Tate, 1986; Oades and Waters, 1991; Shang and Tiessen, 1998) which indirectly enhances OM stability (Balesdent et al., 2000; Totsche et al., 2017) without necessarily showing proportionality to metal concentrations.

To untangle co-varying factors, Wagai and Mayer (2007) assessed Fe oxide contribution on C storage by quantifying the C released during the reductive Fe oxide dissolution with dithionite for soils covering eight soil orders. After correcting for the OC release due to salt and extractive pH effects, the study conservatively estimated that 2-25% (up to 60% for a highly-weathered, Fe-rich soil) of total soil OM was Fe-bound and the C:Fe ratio of the extracts suggested greater contribution of precipitated organo-metal complexes than simple adsorptive association in lower pH soils. Subsequent dithionite-based studies confirmed that less than half (typically less than a quarter) of total OM were associated with Fe in a range of soils and sediments (Coward et al., 2018; Coward et al., 2017; Lalonde et al., 2012; Zhao et al., 2016). Wagai et al. (2013) further examined the potential contribution of other metal phases such as short-range-order minerals, organo-metal complexes, and their coprecipitates using other extractants and showed that, even as liberal estimates, 5-60% of total OM in a range of acidic to near neutral soils (higher percentages for volcanic soils and spodic horizons) could be explained by direct association with Fe and Al phases. The limited extractability of OM with these metal phases implied the potentially critical role of physical protection via ternary associations of OM, metals, and clay (Wagai and Mayer, 2007). More recent studies showed that a portion of soil Fe phases in soil can be protected from reductive dissolution (dithionite extraction) due presumably to physical protection within microaggregates or co-precipitation with short-range-order aluminosilicates (Coward et al., 2018; Suda and Makino, 2016; Filimonova et al., 2016), suggesting both the limitation of single extraction approach and the importance of aggregation/precipitation reactions. On the other hand, experimental studies revealed specific factors and underlying mechanisms behind OM-metal interaction via adsorption, complexation, and co-precipitation using pure metal phases under well-defined laboratory conditions (Chen et al., 2014; Mikutta et al., 2011; Nierop et al., 2002; Schneider et al., 2010; Tamrat et al., 2019; Kaiser, 2003). However, a large knowledge gap still remains between the laboratory studies and field-based studies (see a review by Kleber et al., 2015).

Critical to filling this gap is to identify factors controlling the distribution and localization of different pedogenic metal phases in soil systems because different modes of organo-metal association likely take place at specific local environments. At larger spatial scales, mobilization and accumulation of pedogenic metal phases and their interaction with OM over time and along soil profile depth have been well-recognized (e.g., Kramer et al., 2012; Lawrence et al., 2015). At micro- to nano-meter scales, on the other hand, advanced imaging techniques revealed co-localization of OM and pedogenic Fe and Al in natural soils (Asano et al., 2018; Garcia Arredondo et al., 2019; Inagaki et al., 2020; Wan et al., 2007), although up-scaling of such information remains a major challenge. At horizon or bulk soil scales, physical fractionation studies have indicated the presence

– but not the spatial arrangement – of multiple OM pools of varying turnover rate and degree of mineral associations (Christensen, 2001; von Lützow et al., 2007).

100   Density provides a useful fractionation approach to assess the localization of pedogenic Fe and Al phases because many biogeochemical characteristics of soil particles are closely related to their density (Christensen, 2001; Sollins et al., 2009; Turchenek and Oades, 1979; von Lützow et al., 2007). The density of soil particles is primarily controlled by the relative amounts of the two major components, OM and mineral. The average density of OM present in soil is typically around 1.4 g cm^{-3} but can range between 1.1-1.9 g cm^{-3} across soils and sediments (Mayer et al., 2004). The minerals typically found in

105 soils such as aluminosilicate clays have the density of >2.4 g cm^{-3} including short-range-order allophane and imogolite (2.75 and 2.70 g cm^{-3}, Wada, 2018) with minor exceptions such as phytoliths (2.1-2.15 g cm^{-3}, Drees et al., 1989). Among metal oxides, Fe oxides have much higher densities (3.8-5.3 g cm^{-3}, Cornell and Schwertmann, 2003) compared with Al hydroxides such as gibbsite (2.4 g cm^{-3}, Anthony et al., 1997). Pedogenic metals can remain as distinct phases, or they can associate with OM or other minerals. From the perspective of OM, both pedogenic metals and other minerals will be found in a high-density

110 fraction (>2.4 g cm^{-3}) unless they associate with OM. While OM binding lowers the density of Fe and Al phases in laboratory (Kaiser and Guggenberger, 2007), its extent under various pedogenic environments is virtually unstudied.

      We hypothesize that most pedogenic metals are found in <2.4 g cm^{-3} density fractions regardless of soil type due to their high reactivity with OM. Because of the higher density and redox sensitivity, pedogenic Fe may concentrate in different density phases from pedogenic Al for any given soils, assuming that organo-Fe and organo-Al associations take place independently.

115 Alternatively, if the metal dissolution and subsequent interaction with OM are regulated by the same environmental factors, their distribution along the particle density gradient would be similar. Furthermore, if submicron-sized, OM-rich metal phases act as binding agent as suggested for a volcanic soil based on STXM/NEXAFS and electron microscopy (Asano and Wagai, 2014; Asano et al., 2018), they may preferentially bind with other fine-sized minerals (e.g., clays) to form the ternary associations previously postulated (Wagai and Mayer, 2007). These ideas were tested by fractionating soil particles into 4 to

120 7 density classes after a mild level of dispersion (mechanical shaking in solution) and by quantifying the amounts of Fe and Al phases by selective dissolution techniques that target different metal phases (pyrophosphate, acid oxalate, and dithionite-citrate extractions in sequence) using 23 soil samples from 11 sites spanning 5 climate zones, 5 soil orders (Andisols, Spodosols, Inceptisols, Mollisols, Ultisols), and including several subsurface horizons and both natural and managed (upland and paddy) soils.

125   Terminology: Weathering products of Fe- and Al-bearing minerals during pedogenesis are collectively called as "pedogenic Fe and Al phases" in this study. We use the term "complex" to refer to aqueous organo-metal complexes and their precipitates, and avoid its use to describe broader associations such as organo-clay and organo-mineral complex. Various types of OM-metal association are discussed by grouping into three general mechanisms (adsorption, complexation, and aggregation) while recognizing that organo-metal complexes in soil are mainly coprecipitated with other metal phases and particles. The

130 term "particle" is used in a broad sense to include aggregates as well as single organic or mineral particles.

2 Methods

2.1 Soil sample source

The soil samples selected for this study reflects our primary interest on the soils and soil horizons that hold high OM via its interaction with reactive mineral phases. Soil sample set consisted of four groups: allophanic Andisol (silandic), non-allophanic (aluandic) Andisol, spodic, and crystalline mineralogy group (n=23, Table 1), including both natural and cultivated soils from six climate zones with a wide range of mean annual temperature (5-24 °C) and precipitation (221-2392 mm yr^{-1}).

Allophanic Andisol samples were collected in Kanto plain and Kofu basin, Japan. Parent material is mainly rhyolitic and basaltic volcanic ash deposits. Dominant clay-sized minerals are short-range-order (SRO) minerals – more allophane/imogolite-type minerals than hydrous iron oxides such as ferrihydrite. Minor amounts of gibbsite, kaolinite, chlorite, hydroxyl-interlayered vermiculite, mica, quartz, and feldspar are often found in these soils. Five of the samples were from a long-term field experiment for OM management (A-1 to A-5) and the data from these samples have been reported previously (Wagai et al., 2018). The sample group also includes two pairs of soils (A-6 vs. A-7, and A-8 vs. A-9) from other long-term field experiments of OM amendment and one soil from a relatively undisturbed secondary forest site.

Non-allophanic Andisol samples consist of four horizons from a well-characterized pedon (Pacllic Mdanudand) from Field Science Center of Tohoku University, Miyagi, Japan, located on a gentle slope of a fan in mountain valleys at 190 m elevation maintained as grassland (Sasa nipponica). Parent material is dacitic volcanic tephra with alluvium including smectitic sedimentary rock. A2 horizon contained a key tephra (Hijiori pumce: 10k yr BP).

Spodic group consists from the spodic horizon from two pedons (coarse-loamy, isotic, frigid, Typic Haplorthods, developed from ca 1-m thick glacial till) under coniferous and deciduous forest types in Bear Brooke Watershed, Maine, USA. Further details on the sites and soil OM characteristics can be found in Ohno et al. (2017). Major soil minerals are quartz with moderate amounts of plagioclase, K-feldspar, and hornblende (Swoboda-Colberg and Drever, 1993).

Crystalline mineralogy group consists of a range of soils relatively low in extractable Fe and Al phases or high in more stable clay-sized minerals such as kaolinite. The paddy soil (C-1) has been under seasonal flooding (May to Aug/Sept) for more than several decades. The other two soils (C-2, C-3, classified as Aquic Hapludult) are from long-term experiment of manure application. The most arid soil in our sample set is Mongolian forest steppe soil (C-4), Calcic Kastanonzems in WRB classification system. Our A horizon sample, however, contains no carbonate (Asano et al., 2007). The other three soils are from an elevation gradient under tropical rainforest with the dominant clay mineralogy of kaolinite, gibbsite, hydroxyl-interlayered vermiculite, and quarz (C-5) and illite, kaolinite, and quartz (C-6, C-7). More details on the sites and soils are shown in Wagai et al. (2008) and Tashiro et al. (2018).

All samples were air-dried and 2-mm sieved prior to density fractionation and chemical analyses. Air-drying did not significantly change OM and metal distribution across density fractions, showing no irreversible aggregation by air-drying for an allophanic Andisol (Wagai et al., 2015) and presumably for the other soils. Carbon refers to organic C in this study as no carbonate was found in these soils.

2.2 Physical fractionation by density

We sorted soil particles based on particle density using sodium polytungstate (SPT-0 grade, Sometsu, Germany) to make the liquids of various densities. We employed mechanical shaking to disrupt less-stable aggregates and sequentially separated density fractions following previous studies (Crow et al., 2014; Sollins et al., 2009; Wagai et al., 2018). Most soil samples were separated into 6-7 fractions (n=18) while the other 5 samples (A-6, A-7, A-8, A-9, C-1) examined at a later stage were fractionated into only 4 fractions (Table 1, also see Table A1) because we learned that the main allocation pattern can be captured by four density fractions. The sieved soil samples were mixed with 1.6 g cm^{-3} SPT solution (soil:solution ratio = 10g:40mL), mechanically shaken for 30 min at 120 rpm, and centrifuged (20 min, 2330 g). The floating material (<1.6 g cm^{-3}, the lowest-density fraction, F1) was collected on 0.22 μm membrane filter using a vacuum filtration system. These steps (shaking to centrifugation) were repeated three times to maximize the recovery of this fraction. The materials caught on the filter were washed with deionized water until the salt concentration of the final 50 mL water reached <50 μS cm^{-1} and then transferred to a beaker for oven-drying at 80 °C. After the isolation of F1, the remaining material in the centrifuge tube was re-suspended in 1.8 g cm^{-3} SPT solution, shaken again, and centrifuged. The floating materials (1.6-1.8 g cm^{-3}, F2) were transferred to 250 mL bottles, mixed with deionized water, centrifuged (17,000 g, 30-60 min) and then the supernatant was discarded. This process was repeated 4-5 times until the supernatant salt concentration reached <50 μS cm^{-1} and the rinsed materials were freeze-dried. Following the same procedure, we then sequentially isolated higher-density fractions (e.g., F3:1.8-2.0, F4: 2.0-2.25, F5: 2.25-2.5, and F6: >2.5) using correspondingly higher density SPT solutions. To fully recover each density fraction, we repeated the steps (from shaking to the recovery of floating materials) at least three times.

The selection of cut off density for higher-density fractions varied among the soils (Table A1). This was partly due to soil mineralogical difference (e.g., soils expected to have higher Fe contents had the highest density cut off of 2.75 instead of 2.6 g cm^{-3}). The lowest-density fractions (<1.6 g cm^{-3}) were oven-dried at 80 °C instead of freeze-drying for logistical reason. Due to the concentration of the extractable metals in this fraction, we assumed little effect of the difference in the drying method on our result interpretation. We also assume little impact of sodium polytungstate on the extractability of Fe and Al phases or the nature of soil microaggregates as the SPT solution after the density fractionation typically had the pH value similar to bulk soil pH.

2.3 Extraction of metal phases

Bulk and density-fractionated samples were sequentially extracted by sodium pyrophosphate (PP) followed by acid oxalate in dark (OX) and then by dithionite-citrate (DC) following (Wagai et al., 2018). First, initial PP extraction was conducted at the soil:solution ratio of 100mg:10mL with 0.1 M sodium pyrophosphate (pH=10), and then shaken at 120 rpm for 16 h. After high-speed centrifugation (29,000 g, 45 min), an aliquot of the extract was immediately taken for dissolved C, N, and metal analyses. Second, the residue after discarding the remaining supernatant was re-suspended and extracted with 10 mL of 0.2 M acidified sodium oxalate solution (pH=3.0), shaken at 120 rpm for 4 h in the dark. The conventional acid oxalate

method (Loeppert and Inskeep, 1996) was modified by replacing ammonium oxalate with sodium oxalate to allow the direct quantification of co-dissolved N while achieving the same extraction efficiency of Fe, Al, and Si (Wagai et al., 2013). After the high-speed centrifugation, an aliquot of the extract was immediately diluted for metal and N analyses to avoid precipitation. Third, 0.1 g of sodium dithionite was added to the remaining residue and mixed with 10 mL of 22% (by wt) sodium citrate. The mixture was shaken for 16 h and centrifuged under the same condition as above. All extractions were done at room temperature (20-22 °C). We did not filter the supernatants after the high-speed centrifugation of PP extracts as our pilot test showed no systematic decrease in dissolved organic C and metals by vacuum filtration using 0.025 μm pore-sized membrane (Millipore, VSWP, Bedford, MA, USA). Similarly, no filtration was done for OX and DC extracts after the high-speed centrifugation.

2.4 Chemical analyses

The concentrations of Fe, Al, Si, and Mn in the extracts of PP, OX, and DC were analyzed by inductively coupled plasma-optical emission spectroscopy (Vista-Pro, Agilent, CA, USA). The metal analyses were done for all fractions. The only exception is the lowest-density fraction from three soil samples (A-5, N-4, C-2) where low mass recovery prevented the extractions. Analytical errors associated with our density fractionation were sufficiently low for C, N, and the extractable metals (<12%, Wagai et al., 2015) to allow testing of our hypothesis. When assessing the role of extractable metal as a whole, we summed weight-based concentrations of Al and Fe as "Al + 0.5Fe" to approximately normalize the atomic mass difference between Al and Fe for graphical and statistical purposes. This allows us to compare the metal concentration with C on a weight basis. We also reported some values including the stoichiometric relationships among the target elements (e.g., Al:Si ratio) on a molar basis to allow comparison with other literature values.

Co-dissolved organic C and N by PP extraction and the N by OX extraction were quantified by TOC analyzer (Shimadzu TOC-V/TNM1, Kyoto, Japan). Dissolved organic C (DOC) was measured as non-purgeable organic C after acidification and C-free air purging. Total dissolved N was measured by a chemiluminescence accessory. This method, including the caveats on this technique, was discussed elsewhere (Wagai et al., 2013). Because quantifying the soil C in an oxalate extract is not possible, we estimated the C associated with OX-extractable mineral phases (DOC_{OX}) by multiplying total dissolved N concentration in OX extract by the C:N for each density fraction. This estimation assumes that the OM dissolved by the oxalate extraction has the same C:N ratio as that in bulk fraction. This assumption cannot be fully justified but would be a reasonable approximation for the purpose of assessing the trends because a plot of the C:N ratio of PP-extractable phase against that of bulk soil C:N (regression through the origin) showed a significant positive correlation (r^2=0.89, p<0.0001) with the slope close to one (1.25 with 95% confidence interval of 1.15-1.32). Total organic C and N concentrations in the isolated fractions and bulk samples were analyzed by an elemental analyzer (Flash2000 Thermo Fisher Scientific Inc., USA). All the elemental concentrations from the three extractions conducted were shown in Table A1.

2.5 Extractable elements expressed in two ways

The extractable elements were examined for their concentrations within each density fraction and across the fractions. First, we assessed the *concentration* of the elements for each extractable phase per density fraction mass (e.g., mg Fe g^{-1} fraction). Second, we also assessed the *distribution* of the elements per bulk soil mass (e.g., mg Fe g^{-1} bulk soil) by multiplying the elemental concentration per fraction (mg Fe g^{-1} fraction) by the mass proportion for the respective fraction in bulk soil (g fraction g^{-1} bulk soil).

2.6 Peak density determination

For each soil sample, we determined the particle density at which the metal concentration from each extraction was highest (termed as "peak density") using two approaches. First, we simply selected the density fraction where the metal concentration was the highest among the fractions for a given soil and used its midpoint (e.g., 2.1 g cm^{-3} for 2.0-2.2 g cm^{-3} fraction) as the peak density. The actual peak density is not necessarily its mean especially for the samples separated into a smaller number of fractions. Thus, as a second approach, we also estimated the peak density by fitting a normal distribution curve to the metal concentrations per fraction against particle density for each soil (Fig. A1, left panels). The majority of soil samples fitted well, though we had to remove the data points from the lowest- and highest-density fractions in some cases (Fig. A1). For instance, OX and DC-extractable metal concentrations in the highest density fractions were quite high for non-allophanic Andisol samples due presumably to magnetite. Thus, those data points were not used for the fitting. Similarly, we eliminated the lowest one or two density fractions of PP- and OX-extractable metal concentration data from six samples from the crystalline mineralogy group. Eliminating these data points (Fig. A1) was done only to enable fitting a normal distribution (on average r^2= 0.90-0.98, Fig. A2a). The mean of the normal distribution for each extraction/soil was used as the second estimate of peak density. We also determined the mass-weighted particle density at which the metal was most concentrated. After calculating the metal distribution along the density gradient (i.e., [metal concentration] x [mass fraction]), the two approaches above were applied to determine the peak density for each soil sample and each extractable metal phase. A normal distribution fitted well for most samples (Fig. A1 right panels, Fig. A2b).

2.7 Scanning electron microscopy

Isolated density fractions from selected soil samples were observed by SEM (SU1510, Hitachi high-technologies, Tokyo, Japan). Subset of freeze-dried density fractions were re-dispersed in ultrapure water by weak sonication (<10 J mL^{-1}), deposited on carbon tape, and were Pt-Pd coated prior to the observation.

2.8 Statistics

Linear regression analyses between extractable metals and DOC were done using JMP software (version 8.0.1, SAS Institute, Cary, NC. USA). Density-dependent change in the proportion of total C in each fraction explained by the association

with PP- and OX-extractable phases ($[DOC_{PP}+DOC_{OX}]$:TC) was modeled for each soil group using polynomial functions using JMM software.

260

3   Results

3.1 Recovery after sequential density fractionation

Our density fractionation procedure showed a largely reasonable recovery of mass, C, and N for the 23 soil samples studied (Table 2). While the recovery of the metals assessed by PP-, OX-, and DC sequential extractions was generally good,
265   the variation among the soils was larger (Table 2) as some soil samples and metal phases showed poor recoveries. Possible sources of errors are (i) the small sample mass used for the extractions, (ii) additive errors from the sequential extractions, and (iii) the small sizes of targeted pools. For example, the recovery worsened for DC-extractable Al and Si pools following PP and OX extractions. Incomplete removal of colloidal Fe and Al phases likely explains higher metal recovery from Andisol samples ($118 \pm 36\%$) compared to non-Andisol samples ($84 \pm 12\%$) in PP extraction. The factors affecting the poor recovery
270   with the sequential extraction approach were discussed in more detail elsewhere (Wagai et al., 2018). We considered that the obtained recoveries (Table 2) are tolerable for assessing the general patterns of the metals and OM across the density fractions.

3.2 Concentration of C, N, and extractable metals along the particle density gradient

The C concentration was the highest in the lowest-density fraction (238-443 mg C g^{-1} fraction), declined with increasing density up to ca. 2.5 g cm^{-3}, and remained low (1.5-7.1 mg C g^{-1} fraction) at higher densities for each of the studied soils (Fig.
275   A3a). Similarly, C:N ratio showed a progressive decline with increasing density in each soil (Fig. A3b). While the majority of the soil samples showed very low C concentration and C:N ratio in the fractions higher than ca 2.5 g cm^{-3}, a few samples showed a slight increase towards the highest density fraction.

The extractable metal concentration (Al+0.5Fe) generally showed a unimodal pattern along the particle density gradient with some distinct patterns among the four soil groups (Fig. 1, also see Fig. A1 left panels for individual soils). Allophanic
280   Andisol group showed higher OX- and DC-extractable metals ($metal_{OX}$, $metal_{DC}$) especially in a meso (intermediate) density range (1.8-2.4 g cm^{-3}) up to 78.3 mg g^{-1} fraction (1.46 mmol g^{-1} fraction) for $metal_{OX}$ and 27.2 mg g^{-1} fraction (0.38 mmol g^{-1} fraction) for $metal_{DC}$, whereas non-allophanic Andisol and Spodosol groups were characterized by high concentrations of PP-extractable metals ($metal_{PP}$) up to 53.2 mg g^{-1} fraction (1.97 mmol g^{-1} fraction. As expected, the crystalline mineralogy group showed the lowest levels of $metal_{PP}$ and $metal_{OX}$ with moderate amounts of $metal_{DC}$ from highly-weathered soil samples. Two
285   exceptions to the general unimodal pattern were present. For $metal_{PP}$, three soil samples showed their peak metal concentrations at the lowest density. For $metal_{OX}$, three samples of non-allophanic Andisols showed the highest metal (esp. Fe) concentrations at the highest density due presumably to the presence of Fe-bearing primary minerals such as magnetite. Even in the soils relatively low in specific metal phases (e.g., the crystalline mineralogy group low in $metal_{PP}$ and $metal_{OX}$, and the non-

allophanic Andisol and Spodosol groups low in $metal_{OX}$ and $metal_{DC}$), the highest metal concentrations were found at a meso-density range (Fig. A1 left panels).

Similar patterns were shown when assessing the distribution of the metals along the density gradient by accounting for mass distribution (Fig. A1 right panels). The unimodal pattern remains for most samples, indicating that the major portions of respective metal phases accumulated in a meso-density range. However, the dominant metal phase clearly differed among the soil groups. In the allophanic Andisol group, $63 \pm 9\%$ of the total extractable metal was present in OX-extractable phase. On the other hand, the non-allophanic Andisol and Spodosol groups showed that $59 \pm 25\%$ and $75 \pm 14\%$ of the total extractable metals, respectively, were accounted for by PP-extractable phase. In the crystalline mineralogy group, DC-extractable phase accounted for higher portions ($41 \pm 14\%$) of the total extractable metal.

The comparison of extractable Fe and Al among the three extractions generally showed the increasing dominance of low-crystallinity phases (PP- and OX- extractable phases) in lower-density fractions (Fig. A4). The proportion of total extractable Fe present as Fe_{PP} and Fe_{OX} showed clear decline for all four soil groups with a note that the highest-density fractions in Andisol samples due presumably to magnetite. A similar declining trend was found for the extractable Al phases. Although minor in quantity, the extractable Mn also showed a similar pattern to Fe in line with the generally positive correlation between extractable Fe and Mn (data not shown). The extractable Si showed less clear patterns along the density gradient (Fig. A4).

The Al:Fe molar ratio was the highest in $metal_{PP}$ phase (4.7 ± 4.3, mean $\pm$ SD) followed by $metal_{OX}$ phase (2.6 ± 1.9) and, expectedly, lowest in $metal_{DC}$ phase (0.4 ± 0.3) across all soils and their fractions. Several patterns were identified (Fig. A5). First, relative enrichment of Fe in $metal_{OX}$ and $metal_{DC}$ phases was evident in the highest density fractions due presumably to the dissolution of crystalline Fe oxides. Second, from the low to meso density up to 2.3 g cm^{-3}, the Al:Fe ratio remained relatively constant with some exceptions. The allophanic Andisol group showed relative Al enrichment at around 1.8 g cm^{-3} for PP-extractable phase and at around 2.0-2.3 g cm^{-3} for $metal_{OX}$ phase. The non-allophanic Andisol group showed the Al enrichment towards low density for all extractable phases. For the other soil groups, similar Al enrichment was found in some samples while others showed constant Al:Fe ratios. Nevertheless, the density at which the metal concentration was the highest among the fractions (i.e., peak density) was quite similar between Fe and Al (Table A1). We thus examined the extractable Fe and Al together (i.e., Al+0.5Fe) for most of the subsequent analyses.

The extractable Al in most soils and fractions was more enriched relative to the corresponding extractable Si. The Al:Si molar ratio was 9.6 ± 16.9 (mean $\pm$ SD) for $metal_{PP}$, 3.6 ± 2.1 for $metal_{OX}$, and 1.1 ± 0.9 for $metal_{DC}$ phase. Concerning density-dependent patterns, the Al:Si ratio in PP- and OX-extractable phases was higher at lower-density fractions for the non-allophanic Andisol and Spodosol groups whereas a weak opposing trend was shown in DC-extractable phase in the crystalline mineralogy group (Table A1).

We further compared the peak location in the unimodal metal concentration patterns along the density gradient among the studied soils (Fig. 1, Fig. A1 left panels). While the peak densities for all extractable metals were found at a meso density range for all soil samples studied, we found important differences among the extractable phases. The peak densities of $metal_{PP}$ phase were more variable compared to $metal_{OX}$ and $metal_{DC}$ phases (Fig. 2). In particular, two C-rich soils (C-3, C-7) had the

fitted peak density of metal$_{PP}$ at <1.5 g cm^{-3} (Fig. A1). The medians (and lower/upper quartiles) of the measured peak density among the 23 soil samples for PP-, OX- and DC-extractable metal phases were 1.7 (1.7-2.0), 2.1 (2.1-2.3), and 2.2 (2.1-2.3) g cm^{-3}, respectively (Fig. 2). Similarly, their means were 1.8, 2.2, and 2.2 g cm^{-3}. The peak densities estimated by the normal distribution fitting also showed comparable values. Thus, the peak densities of all three extractable phases were <2.3 g cm^{-3}. The metal$_{PP}$ phase showed its peak consistently lower by 0.3-0.4 g cm^{-3} than metal$_{OX}$ and metal$_{DC}$ phases (Fig. 1 and 2).

The concentrations of C co-dissolved during the initial PP and subsequent OX extractions (DOC$_{PP}$ and DOC$_{OX}$) correlated positively with the extractable metal concentrations (Fig. 3a-f). Coefficients of determination were highest for Al$_{PP}$+0.5Fe$_{PP}$ (r^2=0.75, p <0.0001) followed by Al$_{PP}$ (0.66, <0.0001) and then Fe$_{PP}$ (0.56, <0.0001). Importantly, the positive DOC$_{PP}$-Al$_{PP}$ and/or DOC$_{PP}$-Fe$_{PP}$ relationship persisted across the density fractions within each soil although the correlation was not significant for 5 out of the 23 soil samples (Fig. A6). The DOC$_{PP}$:Al$_{PP}$ mass ratio (i.e., slope of the regression lines) ranged from 2.9 to 28.2 (mean: 7.9, SE: 1.6) which is equivalent to the mean molar ratio of 17.8 (SE: 14.6).

Similarly, the organic matter co-dissolved by the oxalate extraction (DOC$_{OX}$) was positively related to metal$_{OX}$ owing largely to the allophanic Andisol samples (Fig. 3d-f). Simple linear regression of DOC$_{OX}$ against Al$_{OX}$, Fe$_{OX}$, and Al$_{OX}$+0.5Fe$_{OX}$ concentrations among all samples showed the strongest control by Al$_{OX}$ (r^2=0.66) followed by Al$_{OX}$+0.5Fe$_{OX}$ (r^2=0.60) and then Fe$_{OX}$ (r^2=0.39, p <0.0001). When assessed for individual soils, the positive C-metal relationship (mostly only with Al$_{OX}$) persisted for 8 out of the 14 Andisol samples but no positive relationship was present for the rest of soils (Fig. A7). The range for DOC$_{OX}$:Al$_{OX}$ mass ratio the eight samples was 0.13-0.34 (molar DOC$_{OX}$:Al$_{OX}$ ratio of 0.29-0.76) and that of DOC$_{OX}$:(Al$_{OX}$+0.5Fe$_{OX}$) was 0.11-0.22 (molar DOC$_{OX}$:Al$_{OX}$+Fe$_{OX}$ ratio of 0.26-0.49) for these Andisol samples (data not shown). These ratios were roughly 10-50 fold lower than that from PP-extractable phase.

The proportion of total C in each density fraction co-dissolved by initial PP and subsequent OX extractions (expressed as the sum of PP and OX extractable C) showed an increasing trend with increasing particle density (Fig. 4). Despite high variability especially towards higher density fractions, the increasing trend with density was fitted by a polynomial curve for each of the four soil groups separately (Table A2). The three soil groups having high extractable metals tended to have higher proportions of extractable C compared to the crystalline mineralogy group. The allophanic Andisol group, which was characterized by higher Al$_{OX}$ and Fe$_{OX}$ concentrations, showed that appreciable amounts of OM were co-dissolved by the dissolution of metal$_{OX}$ phase (Fig. 4a). In contrast, the non-allophanic Andisols and Spodosol groups showed that nearly all the extractable C was released by the initial PP extraction. The non-allophanic Andisol group having characteristically high Al$_{PP}$ and Fe$_{PP}$ concentrations showed that a quarter up to nearly all of the C present in the higher-density fractions was co-dissolved by the initial PP extraction (Fig. 4b).

3.3 Distribution of mass, organic matter and extractable metal phases along the density gradient

The density fraction which accounted for the largest portion of bulk soil mass was in 2.2-2.6 g cm^{-3} density range and its median (and lower-upper quartiles) was 2.5 (2.2-2.6) g cm^{-3} among the 23 soil samples (Fig. 5). Carbon distribution, calculated by multiplying the C concentration by the fractional mass for each density fraction, showed its peak in significantly lower yet

still meso density range (Fig. 5) with the median of 2.1 (1.9-2.2) g cm^{-3}. The data points at 1.4 g cm^{-3} were from three samples (A-1, S-1, and C-7) having very high total C values due to high OM input or reduced decomposition under cooler climate.

The extractable metals were also mainly concentrated in the meso-density range (Fig. A1 left, Fig. 5b), which is statistically indistinguishable from C peak as a whole sample set (n=23). The medians (and lower-upper quartiles) of the peak

360 density for PP-, OX-, and DC-extractable phases were 2.1 (2.1-2.2), 2.1 (2.1-2.3), and 2.2 (2.1-2.4) g cm^{-3}, respectively. In contrast with the concentration-based patterns (Fig. 2), no clear difference was found between PP- and the other two extractions due to the small mass contribution of the lower-density fractions where PP-extractable metal concentration was higher (Fig. A1a).

3.4 SEM observation of meso-density fractions

365 A clear shift in dominant particle type from plant detritus (POM) in the lowest-density fraction to aggregated particles in meso-density fractions, finally to coarse mineral grains in the highest-density fraction was observed for the three selected soils, one from the Spodosol and two from the crystalline mineralogy group (Fig. 6). The size of these particles ranged from a few tens to hundreds μm in diameters. Similar density-dependent changes were previously observed for one of the allophanic Andisols (A-3, Table 1, Wagai et al., 2014). Four density fractions (1.8-2.6 g cm^{-3}) where the majority of metals and OM

370 reside were assessed by SEM in detail. In all three soils, 1.8-2.0 g cm^{-3} and 2.0-2.2 g cm^{-3} fractions were more abundant in fragmented POM which was mostly enmeshed in aggregates or coated with clay-size grains (Fig. 6a, b, e, f, i, j) while the materials in 2.2-2.4 g cm^{-3} fraction appeared largely aggregated with no visible POM (Fig. 6c, g, k). At a closer look at the surface of these aggregates and POM, clay platelet like features (<5 μm) were visible (Fig. 6a-k, magnified views). The next heavier fraction (2.4-2.6 g cm^{-3}) was more abundant in coarser mineral grains with clean surfaces although some grains in this

375 fraction were aggregated or showed rough surfaces (Fig. 6d, h, l, magnified views).

4 Discussion

4.1 Fe and Al phases extracted by the three reagents

The metals released by PP, OX, and DC extractions only *roughly* correspond to specific metal phases present in the soil as these extractions are not highly selective (Parfitt, 2009; Rennert, 2019). This approach, nevertheless, remains important as

380 the extractable metal contents often show significant correlation with soil C storage and turnover times (Masiello et al., 2004; Percival et al., 2000; Porras et al., 2017; Torn et al., 1997; Wada and Higashi, 1976). It is thus critical to elucidate the nature of these metal phases including their localization, which aids resolving the gap between commonly-used mathematical models and the current understanding of soil C dynamics (Blankinship et al., 2018). Compared to common single extraction, a sequential extraction approach may allow better assignments of different Fe and Al phases (Dai et al., 2011; Shang and Tiessen,

385 1998). It is generally assumed that the PP extraction mainly dissolves organo-metal complexes (Bascomb, 1968; Takahashi

and Dahlgren, 2016), whereas the OX and DC extractions target dissolution of short-range-order minerals and crystalline iron oxides, respectively (e.g., Inagaki et al., 2020; Lawrence et al., 2015; Shang and Tiessen, 1998). Pyrophosphate extraction data requires particularly cautious interpretation due to the OM dissolution by high alkalinity (pH 10) and the dispersion or dissolution of colloidal and low-crystallinity Fe and Al oxide phases (Coward et al., 2018; Kaiser and Zech, 1996; Lawrence et al., 2015; Schuppli et al., 1983; Shang and Tiessen, 1998; Wagai et al., 2013). However, the significant DOC_{PP}-$metal_{PP}$ (esp. DOC_{PP}-Al_{PP}) correlations found across the soils (Fig. 3a-c) and, to a limited extent, among the fractions within soils (Fig. A6) imply the predominance of strong OM-metal association phases such as organo-metal complexes in PP extracts because the potential artifacts, if occurring significantly, would have prevented the emergence of such proportional relationship. Most of the studied soils showed significant C-metal correlation with high DOC_{PP}:Al_{PP} molar ratios (mean $\pm$ SE: 17.8 ± 3.5, range: 6.6-63.3) and DOC_{PP}:Fe_{PP} ratios (75.6 ± 18.0, 17.6-168, Fig. A6) in agreement with previous studies (Heckman et al., 2018; Wagai et al., 2013). While C:metal ratios of synthesized organo-metal associations vary widely depending on experimental conditions, higher ratios indicate the dominance of organo-metal complexes over adsorptive association with metal oxides (Wagai and Mayer, 2007). In laboratory coprecipitation experiments, the C:Fe molar ratio exceeding one led to organic encapsulation of Fe oxide particles (Kleber et al., 2015). Takahashi and Dahlgren (2016) estimated the C:metal molar ratio of 8.3 for organo-metal complexes in Andisols. We thus regard the PP-extractable phase as a mixture consisting largely of organo-metal complexes and their coprecipitates with varying amounts of alkali-soluble or desorbable OM and non-centrifugeable colloidal Fe/Al oxide phases.

The OX-extractable metal phase is more likely influenced by short-range-order minerals (Parfitt and Childs, 1988; Rennert, 2019). We found strong positive correlation between Al_{OX} and Si_{OX} (r^2=0.76-0.99) with relatively constant slope: the Al_{OX}:Si_{OX} molar ratio was 2.05 (allophanic Andisols), 2.25 (non-allophanic Andisols), 3.58 (Spodosols), and 3.91 (crystalline mineralogy group). Short-range-order aluminosilicates commonly found in Andisols and Spodosols have a molar ratio of 1-2, but possibly up to 4 for Al-rich allophane (Dahlgren et al., 1993). The OX-extractable phase in the studied soil fractions may also contain poorly-crystalline gibbsite which can form rapidly in OM-rich, acidic soil environment (e.g., Heckman et al., 2013). The source of Al_{OX} and Si_{OX} in the crystalline mineralogy group is less clear but likely to include interlayer components of 2:1 clay such as hydroxy Al polymers and aluminosilicates (Barnhisel and Bertsch, 1989; Wada and Kakuto, 1983) as well as amorphous gibbsite and silica (Drees et al., 1989). Most Fe_{OX} phase is attributable to ferrihydrite and colloidal goethite for lower-density fractions, and less-crystalline Fe oxides as well as magnetite - a primary mineral that associates little with OM due to the lack of hydroxylated surface - for higher density fractions - for higher density fractions (Cornell and Schwertmann, 2003; Parfitt and Childs, 1988; Rennert, 2019). The DC-extractable metal phase obtained after PP and OX extractions largely represents crystalline iron oxides and coprecipitated Al phases (Cornell and Schwertmann, 2003).

The sequential extraction results along the particle density gradient showed that greater proportions of total extractable Fe and Al were present as low-crystallinity phases (e.g., organic complexes, short-range-order minerals) in lower-density fractions (Fig. A4), which agrees well with the high affinity of these reactive phases to complex, coprecipitate, and adsorb OM (Kaiser and Guggenberger, 2003; Kleber et al., 2015; Wagai and Mayer, 2007; Wagai et al., 2013). The Al:Fe molar ratio of the

420 extracts was relatively constant along the particle density gradient in some of the soils (Fig. A5), implying coprecipitation of organo-Fe and organo-Al phases. The other soils, mostly in Andisol and Spodosol groups, showed density-dependent patterns. Some of the allophanic Andisol samples, all of the non-allophanic Andisol samples and one of the two Spodosol samples showed higher Al:Fe ratios towards lower-density fractions especially in $metal_{PP}$ and $metal_{OX}$ phases (Fig. A5a-c). These higher Al:Fe ratios may be explained by higher capability of Al ions to form insoluble complex with organic ligands under low pH

425 and low metal:C ratio conditions (Nierop et al., 2002). In addition, the lower density of organo-Al coprecipitates (1.7 g cm^{-3}) than that of organo-Fe ones (2.5 g cm^{-3}, Kaiser and Guggenberger, 2007) may account for the observed higher Al:Fe ratios.

4.2 Pedogenic metal enrichment at meso-density range

The concentrations of extractable metal phases peaked at meso (intermediate) densities along the soil particle density gradient (Fig. 2, Fig. A1 left panels). Their dominance below the density cutoff of 2.4 g cm^{-3} is explained only by their

430 association with OM which has a much lower density (~1.4 g cm^{-3}), supporting our hypothesis. While the cutoff densities are somewhat arbitrary, we define the range between 1.8 and 2.4 g cm^{-3} as "meso density" for following reasons: (i) a strong decline in OM concentration and C:N ratio above ~1.8 g cm^{-3} (Fig. A3a,b) suggests a major shift in OM source from plant detritus to microbially-altered compounds as shown previously (e.g., Baisden et al., 2002), (ii) both the concentrations and distributions of the extractable metals began to increase at >1.8 g cm^{-3} (Fig. A1), and (iii) most soil minerals have density >2.4

435 g cm^{-3} (see Introduction). Thus, the meso-density fractions are characterized by enrichment of pedogenic Fe and Al phases and their association with microbially-altered OM. The extractable metal phases in the meso densities made up less than one-fifth of soil masses and the rest consisted largely of other minerals (e.g., crystalline clays) to form microaggregates resistant to mechanical shaking (Fig. 6). The meso-density enrichment of the metals thus implies their preferential association with OM relative to the other minerals.

440 Within the meso-density range, we found clear localization of different metal phases. The peak density of $metal_{PP}$ concentration had the median of 1.8 (1.7-2.0) g cm^{-3} which was lower by 0.3-0.4 g cm^{-3} (on average) relative to $metal_{OX}$ and $metal_{DC}$ across the soils (Fig. 2, Fig. A1 left). This difference remained the same when assessing Fe and Al separately. The lower peak density of $metal_{PP}$ can result either from the inherent low density of this phase as indicated by the high C:metal ratios (see Section 4.1, Fig. 3a-c) or from its attachment to low-density particles. The latter implies that the $metal_{PP}$ phase was

445 preferentially associated with lower-density particles such as clay-covered POM (Fig. 6a, c), which would account for the presence of Fe_{PP} phase despite its higher density than Al_{PP} phase.

Progressive changes in the concentrations of both organic and inorganic (mineral) phases along the density gradient (Fig. 1, Fig. A3a) are depicted for an idealized soil (Fig. 7a). While distinguishing between plant-derived POM in low-density fraction and mineral-associated OM (MAOM) in high-density fraction within bulk soil is a critical first step (Lavallee et al.,

450 2020; Sollins et al., 1999), the transition from POM to MAOM is rather continuous and the latter contains a wide array of OM-mineral associations (Hatton et al., 2012; Jones and Singh, 2014; Sollins et al., 2009; Turchenek and Oades, 1979; Wagai et al., 2018) as conceptualized in "Soil Continuum Model" of soil OM formation (Lehmann and Kleber, 2015). The higher-

density fractions (e.g., >2.4 g cm^{-3}) are increasingly dominated with primary minerals and Fe-bearing minerals including crystalline Fe oxides (Jones and Singh, 2014; Sollins et al., 2009) with small amounts of N-rich OM (Fig. A3b). The lower-density fractions, on the other hand, hold increasing amounts of POM with appreciable levels of PP-extractable organo-metal phases especially at around 1.8 g cm^{-3} range (Fig. 1, 2). In the meso-density fractions (1.8-2.4 g cm^{-3}), where the major portions of OM and extractable metals were located, significant portions (20% up to nearly 100%) of the OM therein were co-dissolved by PP and OX extractions (Fig. 4). By applying similar sequential extraction method to four soil profiles of contrasting mineralogy, Heckman et al. (2018) reported, on average, 70% of total C was extractable. These extractable OM possibly existed in metal-bound forms (Coward et al., 2017; Wagai et al., 2013; Zhao et al., 2016). The remaining, non-extractable OM in the meso-density fraction is presumably stabilized by mechanisms other than simple adsorptive association with the extractable metal phases.

4.3 Organo-metal association, aggregation, and OM stabilization

Organo-metal associations take place at multiple spatial scales within a bulk soil. Organo-metallic complexation, sorption, and co-precipitation occur at molecular to colloidal scales (Kleber et al., 2015). Current density fractionation results, on the other hand, suggest that the extractable metals and associated OM contribute to the formation of meso-density aggregates having a few tens to hundreds of μm in diameter (Fig. 6). At the aggregate scale, organo-mineral interactions occur with much higher level of complexity (Keil and Mayer, 2014; Totsche et al., 2017). Here, we discuss how colloidal-scale interaction of metals and OM may be linked with micron-scale aggregate formation to account for the observed density-dependent patterns.

The observed proportionality between extractable metal phases and associated OM among the density fractions gives some hints to bridge between the colloidal and larger-scale associations. Significant C-metal correlations in PP- and OX-extractable phases, previously found across a range of bulk soils (Wagai et al., 2013), were shown among the density fractions (Fig. 3) and even within each soil in many cases (Fig. A6, A7). Specifically, positive DOC$_{PP}$-metal$_{PP}$ correlation (largely DOC$_{PP}$-Al$_{PP}$) was found for all soils except for three samples from the crystalline mineralogy group (Fig. A6) while such correlation for the subsequent OX extraction was limited to 8 out of the 14 Andisol samples (Fig. A7). Relatively constant C:metal ratios across the density fractions imply that the organo-metal association formed in the field remained intact as a physical unit during the fractionation steps and these units were distributed among the fractions. These organo-metal units themselves are presumably present as colloid-sized "nanocomposites" (Fig. 7b) consisting of precipitated organo-metal complexes (i.e., metal$_{PP}$ phase) and, at least in the case of Andisols, OM-sorbed metal oxides (i.e., metal$_{OX}$ phase), such as those identified in soils using high resolution imaging techniques (Asano et al., 2018; Wen et al., 2014). Another feature is that these nanocomposites must be attached to larger particles containing some combination of low-density OM, high-density mineral, or more of each other. Without sufficient size, Stokes Law predicts that they would have remained in density liquid and lost during the centrifugation step.

We hypothesize that these organo-metal-rich nanocomposites function as a glue or effective binding agent (Asano et al., 2018) and promote ternary associations of OM, metal, and clays (Wagai and Mayer, 2007), as depicted in Figure 7b. In fact,

the meso-density materials were largely present as microaggregates with abundant clays on their surfaces (Fig. 6). For the two soil samples (A-3, C-4) that we further size-fractionated following the density fractionation, 59-84% of the mass in the meso-density fractions consisted of <2 μm sized particles (isolated after maximum dispersion by sonication) that were enriched in the extractable metals relative to bulk samples (unpublished data), in support of our hypothesis. How do these nanocomposites form and function? The Al and Fe are trivalent metals and can act as (monomeric or polynuclear) glue between different organic ligands, particles, and surfaces. An organic particle or coating may stick to a mineral surface via van der Waals interactions, but become aggregated to other organic particles via a polyvalent metal connection. Furthermore, monomeric Fe and Al can form various ternary complexes in the presence of OM and other dissolved inorganic species found in soil solution such as Ca and Si, thereby preventing their polymerization (Adhikari et al., 2019; Tamrat et al., 2019; Yang et al., 2017). These organo-metal-rich mixed-phase nanocomposites, acting as glues (organo-metallic glue hypothesis), can give a mechanistic explanation for the moderately strong C-metal correlations among the density fractions (Fig. 3, Fig. A6, A7) as well as for the dominance of OM, metal, and presumably clay in the meso-density range (Fig. 5, Fig. A1 right panels).

Such micro-scale aggregation can enhance OM stability by reducing the accessibility of microbes, exo-enzymes, and/or e- acceptors (Balesdent et al., 2000; Keil and Mayer, 2014; Lehmann et al., 2007; Sollins et al., 1996). Among the pedogenic metal phases, crystalline Fe oxides (roughly corresponds to metal$_{DC}$ phase) strongly enhance microaggregation particularly in highly weathered soils (e.g., Shang and Tiessen, 1998). This metal phase can protect relatively small amounts of OM for a prolonged time (e.g., Eusterhues et al., 2003; Mikutta et al., 2006). Short-range-order mineral could also contribute to aggregation and thus physical protection of OM within such mineral matrix. Microaggregates in Andisols (esp. metal$_{OX}$-rich ones) show high physical stability (Shoji et al., 1993) even against wet oxidation and reductive dissolution treatments (Churchman and Tate, 1986). Stable ternary associations of OM, low-crystallinity Fe oxide, and microporous allophane in an Andisol has been hypothesized (Filimonova et al., 2016). A portion of soil Fe phase such as low-crystallinity Fe oxyhydroxide, and presumably associated OM, can survive harsh dithionite extraction (Coward et al., 2018), in some cases, due to protective effect of metal$_{OX}$ phases. Even after strong dispersion by sonication (up to 1500 J ml^{-1}), 60-70% of total C and extractable metals in Andisols remained in the meso-density fractions (Basile-Doelsch et al., 2007; Wagai et al., 2015) that were largely present as micron- and submicron-sized aggregates (Asano and Wagai, 2014; Asano et al., 2018). Similarly, the main C storage location in tropical Ferrasols was sonication-resistant particles that were characterized by slightly higher density (2.45-2.8 g cm^{-3}), enrichment of halloysite, and resistance to ~200 yrs of cultivation (Basile-Doelsch et al., 2009). Compared to these metal oxide phases, organo-metal complexes are more labile, for instance, with a change in pH (Takahashi and Dahlgren, 2016). Thus their contribution to aggregation may be lower although this phase can be physically occluded within stable microaggregates. Faster turnover (more ^{14}C enrichment) of PP-extractable C compared to the C associated with other mineral phases (Heckman et al., 2018) as well as the metal$_{PP}$ enrichment at lower density (Fig. 1, 2) support this view. While the relative importance of specific metal phases remains to be elucidated, these extractable metals likely contribute to OM stabilization by promoting aggregation via organo-metallic glues as well as by direct organo-metal interaction via complexation and adsorption.

4.5 Co-localization of metal and microbially-altered OM at meso-density fraction

We further considered the distributions of metal and OM along the density gradient to translate the observed results into field-level processes. Their distributions are determined by two variables: mass distribution and the concentration of the respective elements. The peak density of mass distribution was quite variable among the studied soils (Fig. 5), which will be further examined in our companion study (Kajiura et al., in prep.). Consequently, the peak densities of metal phases were also moderately variable. The mean peak densities of both C and all metal phases were, however, ~2.1 g cm^{-3} (Fig. 5). In fact, the meso-density range (1.8-2.4 g cm^{-3}) accounted for $59 \pm 14\%$ and $64 \pm 15\%$ (mean $\pm$ SD) of total C and N, respectively, among the studied soils. Similarly, more than half of the total extractable metals were in the meso-density range ($65 \pm 17\%$ of Fe$_{PP}$, $63 \pm 15\%$ of Al$_{PP}$, $56 \pm 14\%$ of Fe$_{OX}$, $70 \pm 13\%$ of Al$_{OX}$, $61 \pm 17\%$ of Fe$_{DC}$, and $66 \pm 15\%$ of Al$_{DC}$). The meso-density co-localization of OM and the extractable metals found here thus suggest that metal binding via multiple physicochemical processes discussed above contributes to the stability of pedogenic metal phases against leaching/dissolution and that of OM against biological degradation. Our view is consistent with C and N isotope tracer studies that identified meso-density fractions as the main reservoir of stabilized C across a wide range of soils (Baisden et al., 2002; Crow et al., 2014; Hatton et al., 2012; Sollins et al., 2009; Wagai et al., 2018; Jones and Singh, 2014) with an exception of Fe-rich weathered soils where >2.4 g cm^{-3} fractions store more C due to the abundance of heavy minerals (Jones and Singh, 2014; Sollins et al., 2009).

The co-localization of OM and metals is illustrated for the three forest soils developed through contrasting pedogenesis (Fig. 8). In the tropical Ultisol, DC-extractable phase accounted for greater proportions of total extractable metal than the other two soils (Fig. 8a). Accordingly, this phase explained the majority of the OM extractable by PP, OX, and DC (Wagai et al., 2013). The spodic horizon sample under cooler climate stored more C in lower density fractions and held major portions of metals as PP-extractable phase (Fig. 8b) in agreement with podzolization concept (Lundström et al., 2000). The allophanic Andisol held much higher amounts of extractable metals and C than the other two soils (Fig. 8c). Co-localization at a narrower density range in the Andisol can be attributable to higher contents of organo-metallic glue.

4.5 Implications

The similar distributions of OM and extractable Fe and Al found here (Fig. 5, 8, A1) imply a common set of processes that promote the formation of organo-metal associations across a range of pedogenic environments. Almost all samples showed a unimodal distribution with the peaks in the meso-density range (Fig. 1, 2, and Fig. A1). The three processes operating at a fundamental level are (1) the production of microbially-altered OM from the original low-density plant detritus, (2) the release of metals from high-density, weatherable minerals, and (3) the formation of organo-metal-rich nanocomposites and concurrent incorporation of low- and high-density materials (most importantly, clays) into meso density via their gluing properties – the organo-metallic glue hypothesis (Fig. 8) .

From the organic side, the most consistent change along the particle density gradient was the progressive decline in C:N ratio and OM concentration from low to high-density fractions (Fig. A3), which is generally explained by the shift from POM

to microbially-processed compounds (Baisden et al., 2002; Gunina and Kuzyakov, 2014). Microbially-driven, oxidative depolymerization increases the solubility, the number of ionized functional groups (esp. carboxylic groups), and acidity thereby enhancing the reactivity of remaining OM with metals and mineral surfaces (Heckman et al., 2013; Kleber et al., 2015). The accumulation of the pedogenic metal phases from low to meso density fractions (Fig. 2, Fig. A1) thus suggests that oxidative depolymerization of POM appears to be necessary for the organo-metal associations. From the mineral side, metals released by weathering can readily bind to organic ligands. For instance, negatively-charged bacterial cell surface attracts metal cations, which leads to the nucleation and precipitation of low-crystallinity Fe oxyhydroxides and aluminosilicates (Ferris et al., 1989; Urrutia and Beveridge, 1994). Tamrat et al. (2019) showed nano-sized Fe-Al-Si coprecipitate formation from biotite weathering solution in the presence of low-molecular organic acid (termed as nanosized coprecipitates of inorganic oligomers with organics, "nanoCLICs"). These reactions likely promote the formation of the nanocomposites having a relatively narrow range of OM:metal ratios that can act as relatively persistent glue to bind soil particles, most importantly phyllosilicate clays that themselves strongly bind with OM.

The three processes identified (Fig. 9) are ultimately driven by the factors driving pedogenesis – physicochemical forces (heat, water, acidity) and biological activity. Then the environmental conditions promoting the three processes in balance would lead to local maxima of the organo-metallic glue and meso-density aggregates (see Fig. A8 and the discussion therein). Such condition at the global scale includes acidic soils under wetter climate (Rasmussen et al., 2018) especially with the parent materials that are abundant in weatherable minerals. At the pedon scale, the interface of O/A horizons or the B horizons that experience podzolization would fit with this condition. At smaller scales, micro spots having redox fluctuation and rhizosphere likely promote the organo-metallic glue formation due to the abundance of organic ligands and active dissolution/precipitation of Fe and other mineral phases (Chen et al., 2020; Garcia Arredondo et al., 2019; Keiluweit et al., 2015; Yu, 2018). The current view and the growing evidence on rapid formation of various organo-metal-mineral associations at submicron scale (e.g., Basile-Doelsch et al., 2015; Garcia Arredondo et al., 2019; Heckman et al., 2013) suggest that the concept of soil C saturation and soil's capacity to protect C based on clay and silt contents (e.g., Six et al., 2002) require refinement.

Our results and proposed hypothesis may help to integrate some of the important findings and concepts in the literature. The predominance of stabilized OM in organo-mineral fractions (e.g., <20 µm size class or meso-density range) has been shown by physical fractionation studies (e.g., Christensen, 2001; Six et al., 2000; von Lützow et al., 2007) but the involvement of pedogenic metal phases was much less studied. Protective effects of phyllosilicate clays (e.g., Barré et al., 2014) and pedogenic metal phases (e.g., Porras et al., 2017; Wagai and Mayer, 2007) on OM are likely to occur concurrently, and possibly synergistically, within meso-density microaggregates. Enrichment of certain clay minerals in meso-density fractions (e.g., smectite in a Vertisol, kaolinite in Spodosol and Oxisol, Jones and Singh, 2014) and enhanced physical stability of clay aggregates by goethite particle incorporation (Dultz et al., 2019) support this idea. Aggregate hierarchy concept recognized the role of low-crystallinity mineral phases and microbial compounds as persistent binding agents (Tisdall and Oades, 1982) but not their interaction or formation pathways. With new analytical techniques and methodologies, our understanding of microaggregate formation (e.g., Asano and Wagai, 2014; Lehmann et al., 2007; Totsche et al., 2017) and molecular-scale

interaction of OM, metals, and other inorganic phases (e.g., Chen et al., 2020; Tamrat et al., 2019) is advancing. We believe that a remaining key question is how these molecular-scale interactions are related to soil physical fractions and the formation of hierarchical aggregate structure. The current study provides some insights to this end. Further efforts to fill the scale gap will be important to better understand soil's protective capacity to store OM and for the development of more mechanistic

590 biogeochemical models.

Author contribution

RW designed the experiments that were carried out by all co-authors. KM developed the mathematical approach to assess the density-dependent metal distribution. RW prepared the manuscript with contributions from all co-authors."

595

Acknowledgments

This was was supported by JSPS KAKENHI Grant Numbers 15KK0028, 15H02810, 15KT0036, and 18K05369. We grately thank R. Matsuura (Tokyo Metropolitan Agriculture and Forestry Research Center), K. Maruoka (Saitama Agricultural Technology Research Center), S. Yamazaki (Yamanashi Prefectural Agricultural Technology Center), H. Wakasawa

600 (Shizuoka Prefectural Research Institute of Agriculture and Forestry), M. Kasuya (Aichi Agricultural Research Center), and Y. Hayashi (Wakayama Research Center of Agriculture, Forestry and Fisheries) for kindly sharing soils from their long-term experimental fields. We also thank I.J. Fernandez and T. Ohno (Univ. of Maine), S. Hiradate (Univ. Kyushu) and T. Tanikawa (Univ. Nagoya), K. Kitayama (Univ. of Kyoto) and the Sabah Park for field support and Y. Yaegaki, and C. Hayakawa for laboratory assistance. Comments by L.M. Mayer on an earlier draft are greatly thanked.

605

References

Adhikari, D., Sowers, T., Stuckey, J. W., Wang, X., Sparks, D. L., and Yang, Y.: Formation and redox reactivity of ferrihydrite-organic carbon-calcium co-precipitates, Geochimica et Cosmochimica Acta, 244, 86-98, https://doi.org/10.1016/j.gca.2018.09.026, 2019.

610 Anthony, J. W., Bideaux, R. A., Bladh, K. W., and Nichols, M. C.: Volume III. Halides, Hydroxides, Oxides., Handbook of Mineralogy, Mineralogical Society of America, Chantilly, VA 20151-1110, USA., 1997.

Asano, M., and Wagai, R.: Evidence of aggregate hierarchy at micro- to submicron scales in an allophanic Andisol, Geoderma, 216, 62-74, http://dx.doi.org/10.1016/j.geoderma.2013.10.005, 2014.

Asano, M., Wagai, R., Yamaguchi, N., Takeichi, Y., Maeda, M., Suga, H., and Takahashi, Y.: In Search of a Binding Agent: Nano-Scale Evidence of Preferential Carbon Associations with Poorly-Crystalline Mineral Phases in Physically-Stable, Clay-Sized Aggregates, Soil Systems, 2, 32, 2018.

Baisden, W. T., Amundson, R., Cook, A. C., and Brenner, D. L.: Turnover and storage of C and N in five density fractions from California annual grassland surface soils, Glob. Biogeochem. Cycle, 16, 1117, 10.1029/2001GB001822, 2002.

Balesdent, J., Chenu, C., and Balabane, M.: Relationship of soil organic matter dynamics to physical protection and tillage, Soil and Tillage Research, 53, 215-230, https://doi.org/10.1016/S0167-1987(99)00107-5, 2000.

Barnhisel, R., and Bertsch, P.: Chlorites and hydroxy-interlayered vermiculite and smectite, in: Minerals in Soil Environments, 2nd ed., edited by: Dixon, J. B., Weed, S.B., Soil Science Society of America Book Series, Soil Science Society of America, 729-788, 1989.

Barré, P., Fernandez-Ugalde, O., Virto, I., Velde, B., and Chenu, C.: Impact of phyllosilicate mineralogy on organic carbon stabilization in soils: incomplete knowledge and exciting prospects, Geoderma, 235–236, 382-395, http://dx.doi.org/10.1016/j.geoderma.2014.07.029, 2014.

Bascomb, C. L.: Distribution of pyrophosphate-extractable iron and organic carbon in soils of various groups, Journal of Soil Science, 19, 251-268, 10.1111/j.1365-2389.1968.tb01538.x, 1968.

Basile-Doelsch, I., Amundson, R., Stone, W. E. E., Borschneck, D., Bottero, J. Y., Moustier, S., Masin, F., and Colin, F.: Mineral control of carbon pools in a volcanic soil horizon, Geoderma, 137, 477-489, http://dx.doi.org/10.1016/j.geoderma.2006.10.006, 2007.

Basile-Doelsch, I., Brun, T., Borschneck, D., Masion, A., Marol, C., and Balesdent, J.: Effect of landuse on organic matter stabilized in organomineral complexes: A study combining density fractionation, mineralogy and δ13C, Geoderma, 151, 77-86, http://dx.doi.org/10.1016/j.geoderma.2009.03.008, 2009.

Blankinship, J. C., Berhe, A. A., Crow, S. E., Druhan, J. L., Heckman, K. A., Keiluweit, M., Lawrence, C. R., Marín-Spiotta, E., Plante, A. F., Rasmussen, C., Schädel, C., Schimel, J. P., Sierra, C. A., Thompson, A., Wagai, R., and Wieder, W. R.: Improving understanding of soil organic matter dynamics by triangulating theories, measurements, and models, Biogeochemistry, 140, 1-13, 10.1007/s10533-018-0478-2, 2018.

Chen, C., Dynes, J. J., Wang, J., and Sparks, D. L.: Properties of Fe-Organic Matter Associations via Coprecipitation versus Adsorption, Environmental Science & Technology, 48, 13751-13759, 10.1021/es503669u, 2014.

Chen, C., Hall, S. J., Coward, E., and Thompson, A.: Iron-mediated organic matter decomposition in humid soils can counteract protection, Nature Communications, 11, 2255, 10.1038/s41467-020-16071-5, 2020.

Christensen, B. T.: Physical fractionation of soil and structural and functional complexity in organic matter turnover, Eur. J. Soil Sci., 52, 345-353, 10.1046/j.1365-2389.2001.00417.x, 2001.

Churchman, G. J., and Tate, K. R.: Aggregation of clay in six New Zealand soil types as measured by disaggregation procedures, Geoderma, 37, 207-220, https://doi.org/10.1016/0016-7061(86)90049-2, 1986.

Coleman, K., and Jenkinson, D. S.: RothC-26.3 - A Model for the turnover of carbon in soil, in: Evaluation of Soil Organic Matter Models, edited by: D.S., P., P., S., and J.U., S., Springer, Berlin, Heidelberg, 1996.

Cornell, R. M., and Schwertmann, U.: The Iron Oxides: Structure, Properties, Reactions, Occurences and Uses, 2nd ed., Wiley-VCH, 664 pp., 2003.

Coward, E. K., Thompson, A. T., and Plante, A. F.: Iron-mediated mineralogical control of organic matter accumulation in tropical soils, Geoderma, 306, 206-216, https://doi.org/10.1016/j.geoderma.2017.07.026, 2017.

Coward, E. K., Thompson, A., and Plante, A. F.: Contrasting Fe speciation in two humid forest soils: Insight into organomineral associations in redox-active environments, Geochimica et Cosmochimica Acta, 238, 68-84, https://doi.org/10.1016/j.gca.2018.07.007, 2018.

Crow, S., Reeves, M., Schubert, O., and Sierra, C.: Optimization of method to quantify soil organic matter dynamics and carbon sequestration potential in volcanic ash soils, Biogeochemistry, 1-21, 10.1007/s10533-014-0051-6, 2014.

Dahlgren, R., Shoji, S., and Nanzyo, M.: Mineralogical characteristics of volcanic ash soils, in: Volcanic Ash Soils: genesis, properties, and utilization, edited by: Shoji, S., Nanzyo, M., and Dahlgren, R., Elsevier, 101-143, 1993.

Dai, Q.-x., Ae, N., Suzuki, T., Rajkumar, M., Fukunaga, S., and Fujitake, N.: Assessment of potentially reactive pools of aluminum in Andisols using a five-step sequential extraction procedure, Soil Sci Plant Nutr, 57, 500-507, 10.1080/00380768.2011.598445, 2011.

Drees, R. L., Wilding, L., Smeck, N., and Senkayi, A.: Silica in soils: quartz and disordered silica polymorphs, in: Minerals in Soil Environments, 2nd ed., edited by: Dixon, J. B., Weed, S.B., Soil Science Society of America Book Series, Soil Science Society of America, 913-974, 1989.

Dultz, S., Woche, S. K., Mikutta, R., Schrapel, M., and Guggenberger, G.: Size and charge constraints in microaggregation: Model experiments with mineral particle size fractions, Applied Clay Science, 170, 29-40, https://doi.org/10.1016/j.clay.2019.01.002, 2019.

Eusterhues, K., Rumpel, C., Kleber, M., and Kögel-Knabner, I.: Stabilisation of soil organic matter by interactions with minerals as revealed by mineral dissolution and oxidative degradation, Organic Geochemistry, 34, 1591-1600, https://doi.org/10.1016/j.orggeochem.2003.08.007, 2003.

Ferris, F. G., Tazaki, K., and Fyfe, W. S.: Iron oxides in acid mine drainage environments and their association with bacteria, Chem Geol, 74, 321-330, https://doi.org/10.1016/0009-2541(89)90041-7, 1989.

Filimonova, S., Kaufhold, S., Wagner, F. E., Häusler, W., and Kögel-Knabner, I.: The role of allophane nano-structure and Fe oxide speciation for hosting soil organic matter in an allophanic Andosol, Geochimica et Cosmochimica Acta, 180, 284-302, https://doi.org/10.1016/j.gca.2016.02.033, 2016.

Fujii, K., Hayakawa, C., Inagaki, Y., and Ono, K.: Sorption reduces the biodegradation rates of multivalent organic acids in volcanic soils rich in short-range order minerals, Geoderma 333: 188-199, 2019.

Garcia Arredondo, M., Lawrence, C. R., Schulz, M. S., Tfaily, M. M., Kukkadapu, R., Jones, M. E., Boye, K., and Keiluweit, M.: Root-driven weathering impacts on mineral-organic associations in deep soils over pedogenic time scales, Geochimica et Cosmochimica Acta, 263, 68-84, https://doi.org/10.1016/j.gca.2019.07.030, 2019.

Gunina, A., and Kuzyakov, Y.: Pathways of litter C by formation of aggregates and SOM density fractions: Implications from 13C natural abundance, Soil Biology and Biochemistry, 71, 95-104, http://dx.doi.org/10.1016/j.soilbio.2014.01.011, 2014.

685 Hatton, P.-J., Kleber, M., Zeller, B., Moni, C., Plante, A. F., Townsend, K., Gelhaye, L., Lajtha, K., and Derrien, D.: Transfer of litter-derived N to soil mineral–organic associations: Evidence from decadal 15N tracer experiments, Organic Geochemistry, 42, 1489-1501, https://doi.org/10.1016/j.orggeochem.2011.05.002, 2012.

Heckman, K., Grandy, A. S., Gao, X., Keiluweit, M., Wickings, K., Carpenter, K., Chorover, J., and Rasmussen, C.: Sorptive fractionation of organic matter and formation of organo-hydroxy-aluminum complexes during litter biodegradation in 690 the presence of gibbsite, Geochimica et Cosmochimica Acta, 121, 667-683, https://doi.org/10.1016/j.gca.2013.07.043, 2013.

Heckman, K., Lawrence, C. R., and Harden, J. W.: A sequential selective dissolution method to quantify storage and stability of organic carbon associated with Al and Fe hydroxide phases, Geoderma, 312, 24-35, https://doi.org/10.1016/j.geoderma.2017.09.043, 2018.

695 Inagaki, T. M., Possinger, A. R., Grant, K. E., Schweizer, S. A., Mueller, C. W., Derry, L. A., Lehmann, J., and Kögel-Knabner, I.: Subsoil organo-mineral associations under contrasting climate conditions, Geochimica et Cosmochimica Acta, 270, 244-263, https://doi.org/10.1016/j.gca.2019.11.030, 2020.

Jones, E., and Singh, B.: Organo-mineral interactions in contrasting soils under natural vegetation, Frontiers in Environmental Science, 2, 10.3389/fenvs.2014.00002, 2014.

700 Kaiser, K., and Zech, W.: Defects in Estimation of Aluminum in Humus Complexes of Podzolic Soils By Pyrophosphate Extraction, Soil Science, 161, 452-458, 1996.

Kaiser, K.: Sorption of natural organic matter fractions to goethite (α-FeOOH): effect of chemical composition as revealed by liquid-state 13C NMR and wet-chemical analysis, Organic Geochemistry, 34, 1569-1579, https://doi.org/10.1016/S0146-6380(03)00120-7, 2003.

705 Kaiser, K., and Guggenberger, G.: Mineral surfaces and soil organic matter, Eur. J. Soil Sci., 54, 219-236, 10.1046/j.1365-2389.2003.00544.x, 2003.

Kaiser, K., and Guggenberger, G.: Distribution of hydrous aluminium and iron over density fractions depends on organic matter load and ultrasonic dispersion, Geoderma, 140, 140-146, 10.1016/j.geoderma.2007.03.018, 2007.

Keil, R. G., and Mayer, L. M.: 12.12 - Mineral Matrices and Organic Matter, in: Treatise on Geochemistry (Second Edition), 710 edited by: Holland, H. D., and Turekian, K. K., Elsevier, Oxford, 337-359, 2014.

Keiluweit, M., Bougoure, J. J., Nico, P. S., Pett-Ridge, J., Weber, P. K., and Kleber, M.: Mineral protection of soil carbon counteracted by root exudates, Nature Climate Change, 5, 588-595, 10.1038/nclimate2580, 2015.

Kleber, M., Eusterhues, K., Keiluweit, M., Mikutta, C., Mikutta, R., and Nico, P. S.: Mineral–Organic Associations: Formation, Properties, and Relevance in Soil Environments, in: Advances in Agronomy, edited by: Donald, L. S., Advances in 715 Agronomy, Academic Press, 1-140, 2015.

Kramer, M. G., Sanderman, J., Chadwick, O. A., Chorover, J., and Vitousek, P. M.: Long-term carbon storage through retention of dissolved aromatic acids by reactive particles in soil, Global Change Biology, 18, 2594-2605, 10.1111/j.1365-2486.2012.02681.x, 2012.

Kramer, M. G., and Chadwick, O. A.: Climate-driven thresholds in reactive mineral retention of soil carbon at the global scale, Nature Climate Change, 8, 1104-1108, 10.1038/s41558-018-0341-4, 2018.

Lalonde, K., Mucci, A., Ouellet, A., and Gelinas, Y.: Preservation of organic matter in sediments promoted by iron, Nature, 483, 198-200, 10.1038/nature10855, 2012.

Lavallee, J. M., Soong, J. L., and Cotrufo, M. F.: Conceptualizing soil organic matter into particulate and mineral-associated forms to address global change in the 21st century, Global Change Biology, n/a, 10.1111/gcb.14859, 2020.

Lawrence, C. R., Harden, J. W., Xu, X., Schulz, M. S., and Trumbore, S. E.: Long-term controls on soil organic carbon with depth and time: A case study from the Cowlitz River Chronosequence, WA USA, Geoderma, 247–248, 73-87, http://dx.doi.org/10.1016/j.geoderma.2015.02.005, 2015.

Lehmann, J., Kinyangi, J., and Solomon, D.: Organic matter stabilization in soil microaggregates: implications from spatial heterogeneity of organic carbon contents and carbon forms, Biogeochemistry, 85, 45-57, 10.1007/s10533-007-9105-3, 2007.

Lehmann, J., and Kleber, M.: The contentious nature of soil organic matter, Nature, 528, 60-68, 10.1038/nature16069, 2015.

Loeppert, R. H., and Inskeep, W. P.: Iron, in: Methods of Soil Analysis, edited by: Sparks, D. L., Soil Sci. Soc. Am., Madison, WI, 639-664, 1996.

Lundström, U. S., van Breemen, N., and Bain, D.: The podzolization process. A review, Geoderma, 94, 91-107, https://doi.org/10.1016/S0016-7061(99)00036-1, 2000.

Masiello, C. A., Chadwick, O. A., Southon, J., Torn, M. S., and Harden, J. W.: Weathering controls on mechanisms of carbon storage in grassland soils, Global Biogeochem. Cycles, 18, GB4023, 10.1029/2004gb002219, 2004.

Mayer, L. M., and Xing, B.: Organic Matter–Surface Area Relationships in Acid Soils, Soil Science Society of America Journal, 65, 250-258, 10.2136/sssaj2001.651250x, 2001.

Mayer, L. M., Schick, L. L., Hardy, K. R., Wagai, R., and McCarthy, J.: Organic matter in small mesopores in sediments and soils, Geochimica et Cosmochimica Acta, 68, 3863-3872, 10.1016/j.gca.2004.03.019, 2004.

Mikutta, R., Kleber, M., Torn, M. S., and Jahn, R.: Stabilization of Soil Organic Matter: Association with Minerals or Chemical Recalcitrance?, Biogeochemistry, 77, 25-56, 2006.

Mikutta, R., Zang, U., Chorover, J., Haumaier, L., and Kalbitz, K.: Stabilization of extracellular polymeric substances (Bacillus subtilis) by adsorption to and coprecipitation with Al forms, Geochimica et Cosmochimica Acta, 75, 3135-3154, https://doi.org/10.1016/j.gca.2011.03.006, 2011.

Nierop, K. G. J. J., Jansen, B., and Verstraten, J. M.: Dissolved organic matter, aluminium and iron interactions: precipitation induced by metal/carbon ratio, pH and competition, Science of The Total Environment, 300, 201-211, https://doi.org/10.1016/S0048-9697(02)00254-1, 2002.

750 Oades, J. M., and Waters, A. G.: Aggregate Hierarchy in Soils, Aust. J. Soil Res., 29, 815-828, 1991.

Ohno, T., Heckman, K. A., Plante, A. F., Fernandez, I. J., and Parr, T. B.: 14C mean residence time and its relationship with thermal stability and molecular composition of soil organic matter: A case study of deciduous and coniferous forest types, Geoderma, 308, 1-8, https://doi.org/10.1016/j.geoderma.2017.08.023, 2017.

Parfitt, R. L.: Allophane and imogolite: role in soil biogeochemical processes, Clay Minerals, 44, 135-155, 755 10.1180/claymin.2009.044.1.135, 2009.

Parton, W. J., Schimel, D. S., Cole, C. V., and Ojima, D. S.: Analysis of Factors Controlling Soil Organic Matter Levels in Great Plains Grasslands, Soil Science Society of America Journal, 51, 1173-1179, 10.2136/sssaj1987.03615995005100050015x, 1987.

Percival, H. J., Parfitt, R. L., and Scott, N. A.: Factors Controlling Soil Carbon Levels in New Zealand Grasslands Is Clay 760 Content Important?, Soil Sci. Soc. Am. J., 64, 1623-1630, 10.2136/sssaj2000.6451623x, 2000.

Porras, R. C., Hicks Pries, C. E., McFarlane, K. J., Hanson, P. J., and Torn, M. S.: Association with pedogenic iron and aluminum: effects on soil organic carbon storage and stability in four temperate forest soils, Biogeochemistry, 133, 333-345, 10.1007/s10533-017-0337-6, 2017.

Rasmussen, C., Heckman, K., Wieder, W. R., Keiluweit, M., Lawrence, C. R., Berhe, A. A., Blankinship, J. C., Crow, S. E., 765 Druhan, J. L., Hicks Pries, C. E., Marin-Spiotta, E., Plante, A. F., Schädel, C., Schimel, J. P., Sierra, C. A., Thompson, A., and Wagai, R.: Beyond clay: towards an improved set of variables for predicting soil organic matter content, Biogeochemistry, 137, 297-306, 10.1007/s10533-018-0424-3, 2018.

Rennert, T.: Wet-chemical extractions to characterise pedogenic Al and Fe species – a critical review, Soil Research, 57, 1-16, https://doi.org/10.1071/SR18299, 2019.

770 Schneider, M. P. W., Scheel, T., Mikutta, R., van Hees, P., Kaiser, K., and Kalbitz, K.: Sorptive stabilization of organic matter by amorphous Al hydroxide, Geochimica et Cosmochimica Acta, 74, 1606-1619, 10.1016/j.gca.2009.12.017, 2010.

Schuppli, P. A., Ross, G. J., and McKeague, J. A.: The effective removal of suspended materials from pyrophosphate extracts of soils from tropical and temperate regions, Soil Science Society of America Journal, 47, 1026-1032, 10.2136/sssaj1983.03615995004700050037x, 1983.

775 Shang, C., and Tiessen, H.: Organic matter stabilization in two semiarid tropical soils: Size, density, and magnetic separations, Soil Science Society of America Journal, 62, 1247-1257, 1998.

Shoji, S., Nanzyo, M., and Dahlgren, R.: Volcanic Ash Soils: genesis, properties, and utilization, Developments in Soil Science: 21, Elsevier, Amsterdam, 288 pp., 1993.

Six, J., Merckx, R., Kimpe, K., Paustian, K., and Elliott, E. T.: A re-evaluation of the enriched labile soil organic matter 780 fraction, Eur. J. Soil Sci., 51, 283-293, 10.1046/j.1365-2389.2000.00304.x, 2000.

Six, J., Conant, R. T., Paul, E. A., and Paustian, K.: Stabilization mechanisms of soil organic matter: Implications for C-saturation of soils, Plant and Soil, 241, 155-176, 10.1023/A:1016125726789, 2002.

Smith, P.: Soil carbon sequestration and biochar as negative emission technologies, Global Change Biology, 22, 1315-1324, 10.1111/gcb.13178, 2016.

Sollins, P., Homann, P., and Caldwell, B. A.: Stabilization and destabilization of soil organic matter: mechanisms and controls, Geoderma, 74, 65-105, 10.1016/s0016-7061(96)00036-5, 1996.

Sollins, P., Glassman, C., Paul, E. A., Swanston, C., Lajtha, K., Heil, W., and Elliott, E. T.: Soil carbon and nitrogen: pools and fractions, in: Standard Soil Methods for Long-Term Ecological Research, edited by: Robertson, P., Coleman, D. C., Bledsoe, C. S., and Sollins, P., Oxford University Press, Oxford, 89-105, 1999.

Sollins, P., Kramer, M., Swanston, C., Lajtha, K., Filley, T., Aufdenkampe, A., Wagai, R., and Bowden, R.: Sequential density fractionation across soils of contrasting mineralogy: evidence for both microbial- and mineral-controlled soil organic matter stabilization, Biogeochemistry, 96, 209-231, 10.1007/s10533-009-9359-z, 2009.

Suda, A., and Makino, T.: Functional effects of manganese and iron oxides on the dynamics of trace elements in soils with a special focus on arsenic and cadmium: A review, Geoderma, 270, 68-75, http://dx.doi.org/10.1016/j.geoderma.2015.12.017, 2016.

Swoboda-Colberg, N. G., and Drever, J. I.: Mineral dissolution rates in plot-scale field and laboratory experiments, Chem Geol, 105, 51-69, https://doi.org/10.1016/0009-2541(93)90118-3, 1993.

Takahashi, T., and Dahlgren, R. A.: Nature, properties and function of aluminum–humus complexes in volcanic soils, Geoderma, 263, 110-121, http://dx.doi.org/10.1016/j.geoderma.2015.08.032, 2016.

Tamrat, W. Z., Rose, J., Grauby, O., Doelsch, E., Levard, C., Chaurand, P., and Basile-Doelsch, I.: Soil organo-mineral associations formed by co-precipitation of Fe, Si and Al in presence of organic ligands, Geochimica et Cosmochimica Acta, 260, 15-28, https://doi.org/10.1016/j.gca.2019.05.043, 2019.

Tashiro, Y., Nakao, A., Wagai, R., Yanai, J., and Kosaki, T.: Inhibition of radiocesium adsorption on 2:1 clay minerals under acidic soil environment: Effect of organic matter vs. hydroxy aluminum polymer, Geoderma, 319, 52-60, https://doi.org/10.1016/j.geoderma.2017.12.039, 2018.

Torn, M. S., Trumbore, S. E., Chadwick, O. A., Vitousek, P. M., and Hendricks, D. M.: Mineral control of soil organic carbon storage and turnover, Nature, 389, 170-173, 1997.

Totsche, K. U., Amelung, W., Gerzabek, M. H., Guggenberger, G., Klumpp, E., Knief, C., Lehndorff, E., Mikutta, R., Peth, S., Prechtel, A., Ray, N., and Kögel-Knabner, I.: Microaggregates in soils, Journal of Plant Nutrition and Soil Science, 10.1002/jpln.201600451, 2017.

Turchenek, L. W., and Oades, J. M.: Fractionation of organo-mineral complexes by sedimentation and density techniques, Geoderma, 21, 311-343, 1979.

Urrutia, M. M., and Beveridge, T. J.: Formation of fine-grained metal and silicate precipitates on a bacterial surface (Bacillus subtilis), Chem Geol, 116, 261-280, https://doi.org/10.1016/0009-2541(94)90018-3, 1994.

von Lützow, M., Kögel-Knabner, I., Ekschmitt, K., Flessa, H., Guggenberger, G., Matzner, E., and Marschner, B.: SOM fractionation methods: Relevance to functional pools and to stabilization mechanisms, Soil Biology and Biochemistry, 39, 2183-2207, DOI: 10.1016/j.soilbio.2007.03.007, 2007.

Wada, K., and Higashi, T.: The categories of aluminum- and iron-humus complexes in ando soils determined by selective dissolution, Journal of Soil Science, 27, 357-368, 10.1111/j.1365-2389.1976.tb02007.x, 1976.

820   Wada, K., and Kakuto, Y.: Intergradient vermiculite-kaolin mineral in a Korean Ultisol, Clays and Clay Minerals, 31, 183-190, 1983.

Wada, K.: Allophane and Imogolite, in: Minerals in Soil Environments, 1051-1087, 2018.

Wagai, R., and Mayer, L. M.: Sorptive stabilization of organic matter in soils by hydrous iron oxides, Geochimica Et Cosmochimica Acta, 71, 25-35, 10.1016/j.gca.2006.08.047, 2007.

825   Wagai, R., Mayer, L. M., Kitayarna, K., and Knicker, H.: Climate and parent material controls on organic matter storage in surface soils: A three-pool, density-separation approach, Geoderma, 147, 23-33, 10.1016/j.geoderma.2008.07.010, 2008.

Wagai, R., Mayer, L. M., Kitayama, K., and Shirato, Y.: Association of organic matter with iron and aluminum across a range of soils determined via selective dissolution techniques coupled with dissolved nitrogen analysis, Biogeochemistry, 112, 95-109, 10.1007/s10533-011-9652-5, 2013.

830   Wagai, R., Kajiura, M., Asano, M., and Hiradate, S.: Nature of soil organo-mineral assemblage examined by sequential density fractionation with and without sonication: Is allophanic soil different?, Geoderma, 241–242, 295-305, http://dx.doi.org/10.1016/j.geoderma.2014.11.028, 2015.

Wagai, R., Kajiura, M., Uchida, M., and Asano, M.: Distinctive roles of two aggregate binding agents in allophanic andisols: young carbon and poorly-crystalline metal phases with old carbon, Soil Systems, 2, 29, 2018.

835   Wan, J., Tyliszczak, T., and Tokunaga, T. K.: Organic carbon distribution, speciation, and elemental correlations within soil microaggregates: Applications of STXM and NEXAFS spectroscopy, Geochimica et Cosmochimica Acta, 71, 5439-5449, 10.1016/j.gca.2007.07.030, 2007.

Wen, Y., Li, H., Xiao, J., Wang, C., Shen, Q., Ran, W., He, X., Zhou, Q., and Yu, G.: Insights into complexation of dissolved organic matter and Al(III) and nanominerals formation in soils under contrasting fertilizations using two-dimensional
840   correlation spectroscopy and high resolution-transmission electron microscopy techniques, Chemosphere, 111, 441-449, https://doi.org/10.1016/j.chemosphere.2014.03.078, 2014.

Wieder, W. R., Grandy, A. S., Kallenbach, C. M., Taylor, P. G., and Bonan, G. B.: Representing life in the Earth system with soil microbial functional traits in the MIMICS model, Geosci. Model Dev., 8, 1789-1808, 10.5194/gmd-8-1789-2015, 2015.

845   Yang, J., Liu, J., Hu, Y., Rumpel, C., Bolan, N., and Sparks, D.: Molecular-level understanding of malic acid retention mechanisms in ternary kaolinite-Fe(III)-malic acid systems: The importance of Fe speciation, Chem Geol, 464, 69-75, https://doi.org/10.1016/j.chemgeo.2017.02.018, 2017.

Yu, G.: Root Exudates and Microbial Communities Drive Mineral Dissolution and the Formation of Nano-size Minerals in Soils: Implications for Soil Carbon Storage, in: Root Biology, edited by: Giri, B., Prasad, R., and Varma, A., Springer
850   International Publishing, Cham, 143-166, 2018.

Zhao, Q., Poulson, S. R., Obrist, D., Sumaila, S., Dynes, J. J., McBeth, J. M., and Yang, Y.: Iron-bound organic carbon in forest soils: quantification and characterization, Biogeosciences, 13, 4777-4788, 10.5194/bg-13-4777-2016, 2016.
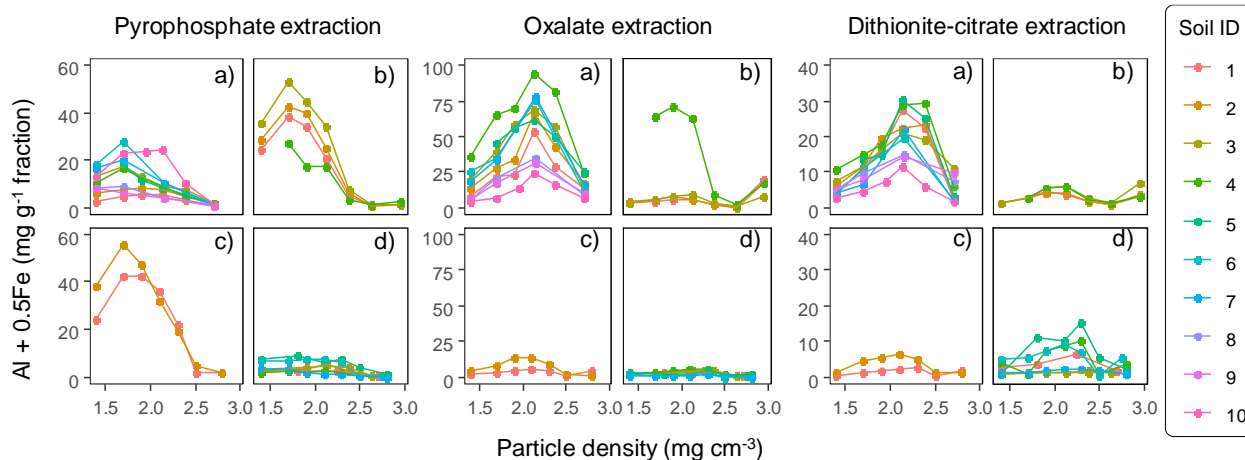
Figures

Figure 1: The concentrations of pedogenic metal (Al+0.5Fe) per fraction along the density gradient for allophanic Andisol group (a), non-allophanic Andisol group (b), Spodosol group (c) and crystalline mineral group (d). The metal extracted by initial
860 **pyrophosphate (left panels), subsequent acid oxalate (central panels), and final dithionite-citrate reagents (right panels) are shown. Each symbol represents individual soil sample. Sample number (1-10) on the right corresponds to sample ID for each soil group in Table 1.**
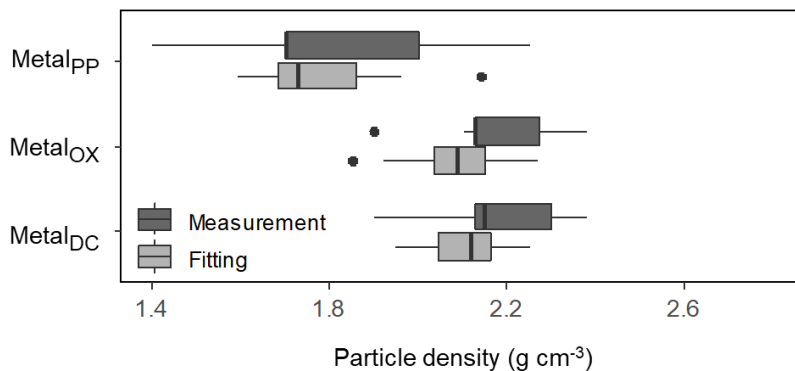
865

Figure 2: Boxplot showing the median and variation of densities at which the concentration of pedogenic metal (Al+0.5Fe) was the highest across the 23 studied soils. The peak density was determined for all three extractions (PP, OX, and DC) for each soil based on measurements (light color) and normal distribution fitting (dark color).

870
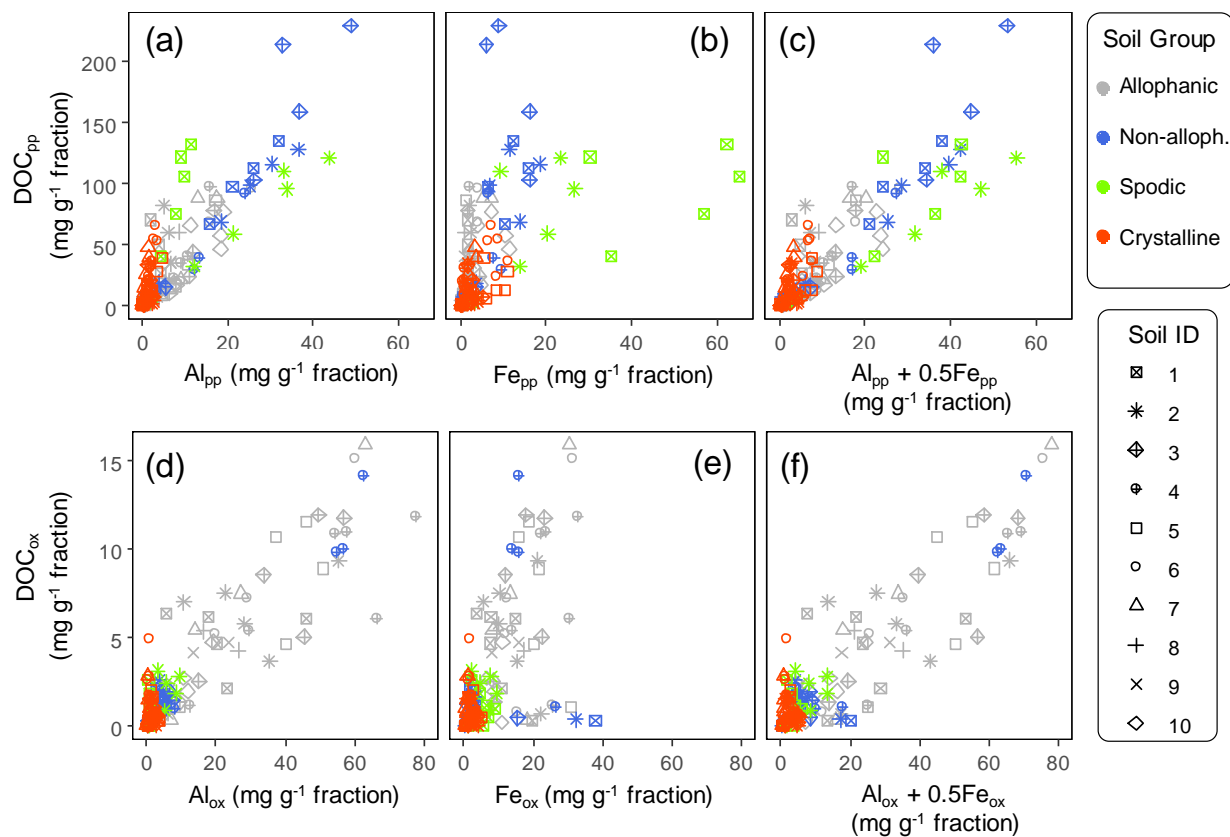
Figure 3: Scatter plot of extractable metals and co-dissolved organic C (DOC) for the density fractions from the studied soils. Pyrophosphate-extractable Al (a), Fe (b), and Al+0.5Fe (c) against DOC_{OX} in upper panel. Oxalate-extractable Al (d), Fe (e), and Al+0.5Fe (f) against DOC_{OX} in lower panel. Symbol color distinguishes the four soil groups and its shape corresponds to sample ID in Table 1.

890
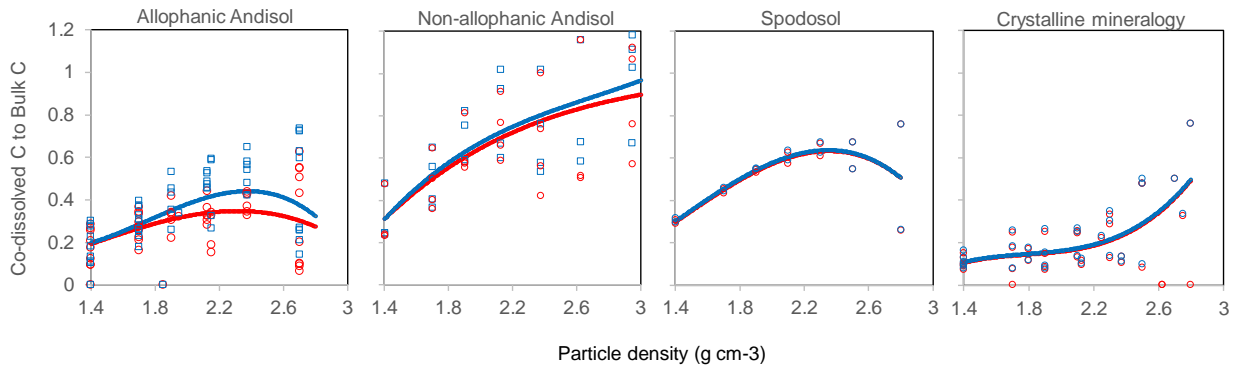
Figure 4: Proportions of bulk C in each density fraction co-dissolved by initial pyrophosphate extraction alone (red circle) and combined with subsequent acid oxalate extraction (blue rectangle), with polynomial fitting curves, for each soil group.

895
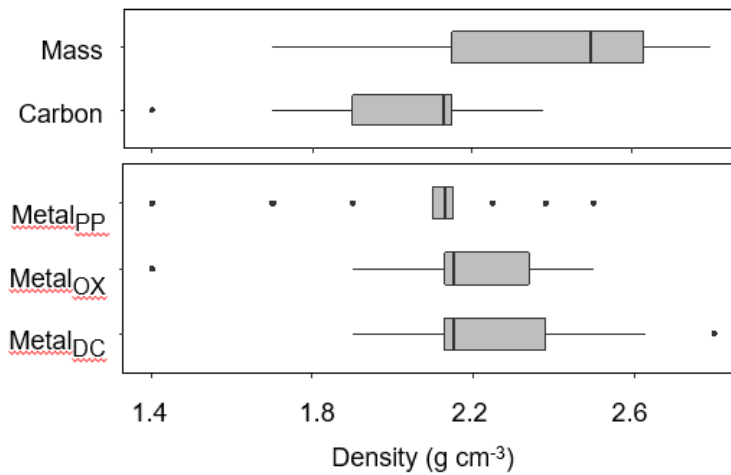
Figure 5: Boxplot showing the median and distribution of the densities at which the distribution of mass, C, and pedogenic metal (Al+0.5Fe) extracted by the three extractants (PP, OX, and DC) were the highest among the 23 studied soils.

900
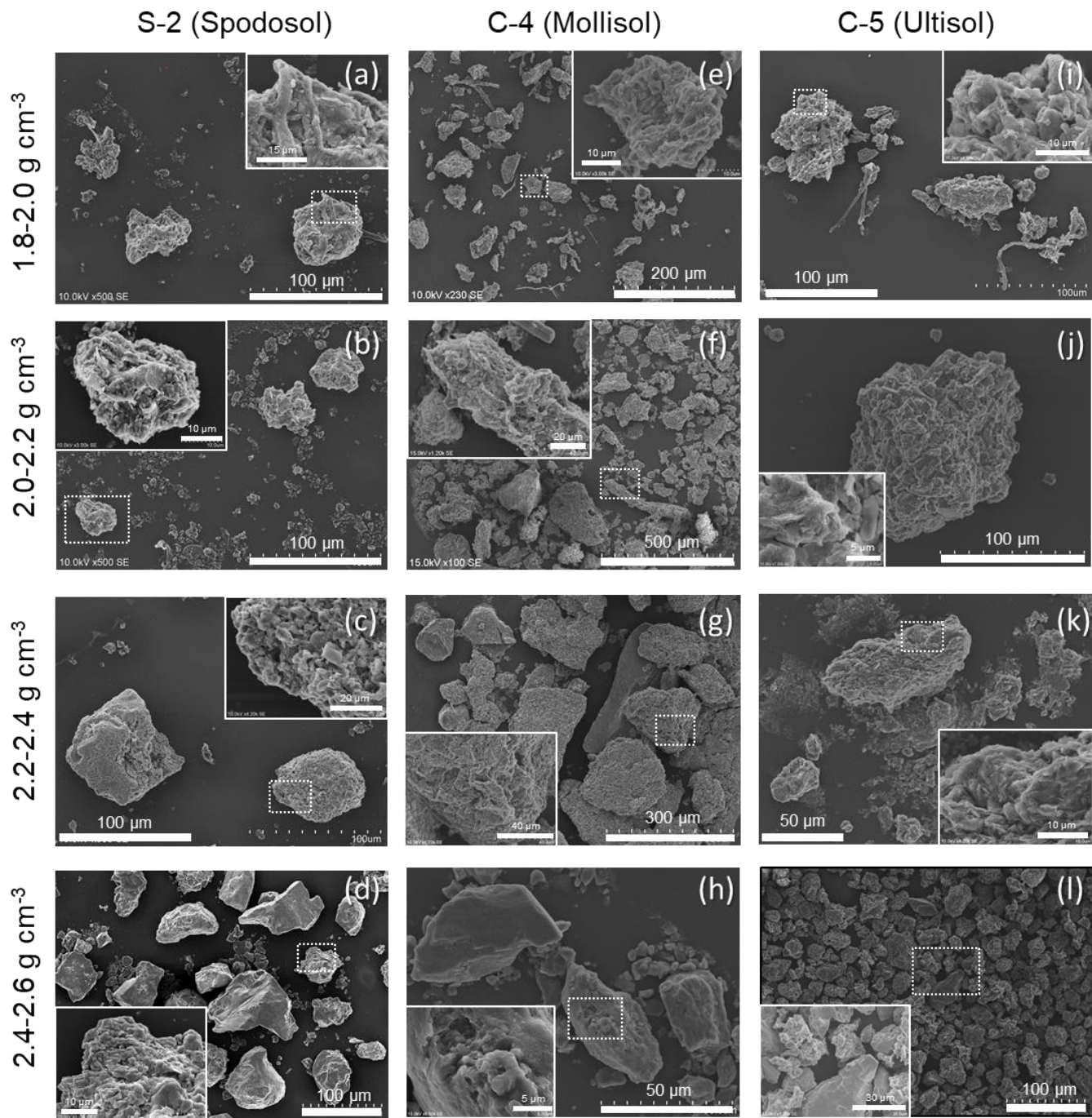
Figure 6: SEM images of three meso-density fractions and the adjacent higher density fraction from S-2 soil (spodic horizon, a-d), C-4 soil (mollic horizon, e-h), and C-5 soil (kaolinitic A horizon, i-l). The enlarged view of the dotted rectangular section is shown at a corner, showing that the surface of selected particles was often aggregated or coated with finer materials such as clay platelets.
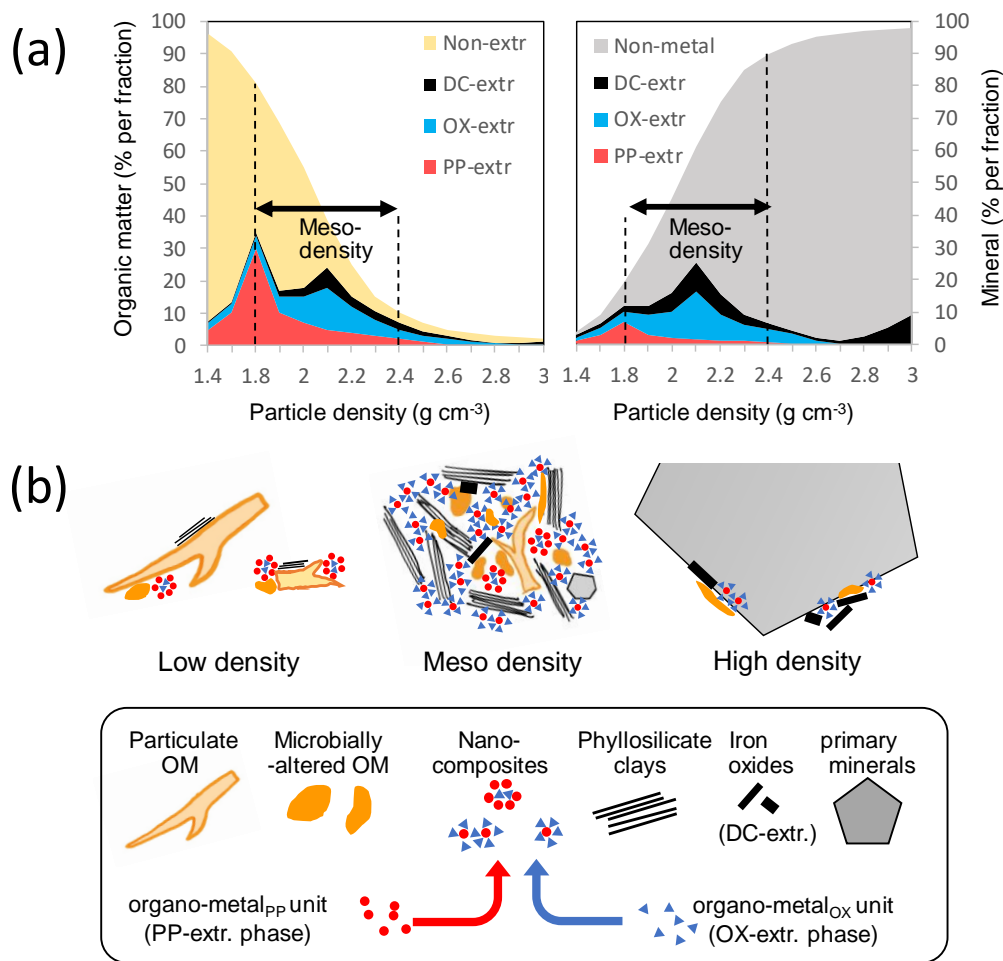
915 **Figure 7: (a) Changes in the concentration of organic and mineral phases along soil particle gradient for an idealized soil. The concentrations of OM (left plot) and metals (right plot) extracted sequentially by pyrophosphate (PP), acid oxalate (OX), and dithionite (DC) per density fraction were shown in different colors. Non-extractable OM includes both particulate and microbially-altered OM. Non-metal mineral phase includes phyllosilicate clays and primary minerals. (b) Schematic representation of low-, meso-, and high-density particles (upper) and their building blocks (lower). PP- and OX-extractable**
920 **phases were presumed to be present as "nanocomposites" that act as glue to form meso-density microaggregates. The distribution of the nanocomposites across density fractions can explain the C:metal proportional relationship found in Fig. 3, A6, and A7. The nanocomposites rich in organo-metal$_{PP}$ unit is more abundant in OM-rich environments (e.g., lower-density fraction) relative to those rich in organo-metal$_{OX}$ units. Objects don't reflect the size difference among them.**

925
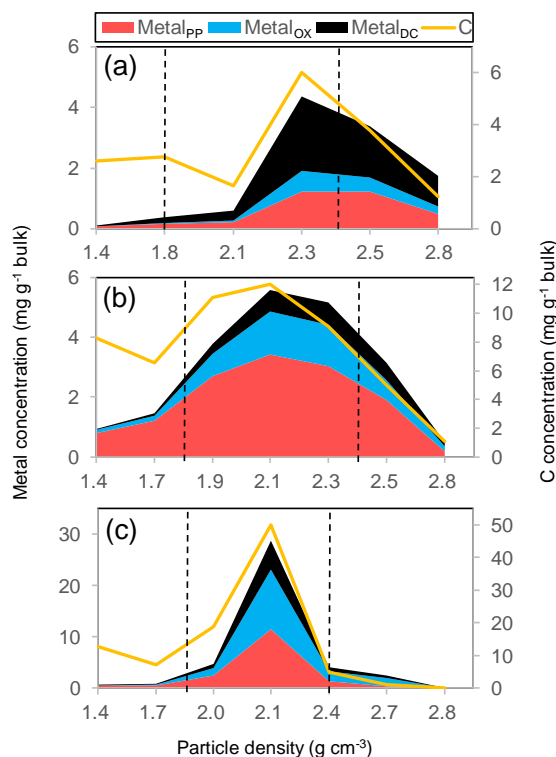
Figure 8: The distribution of the extractable metal phases (Al+0.5Fe) on left Y axis and that of C on the right Y axis along the density gradient for three undisturbed forest soils. A kaolinitic Ultisol (O-5 in Table 1) developed from sedimentary rock under tropical wet climate (a), a Spodosol Bhs horizon (S-2) with quartz and plagioclase rich mineralogy from glacial till under cool temperate moist climate (b), and an allophanic Andisol (A-10) from tephra under warm temperate moist climate (c). Vertical dotted lines show the meso-density range.
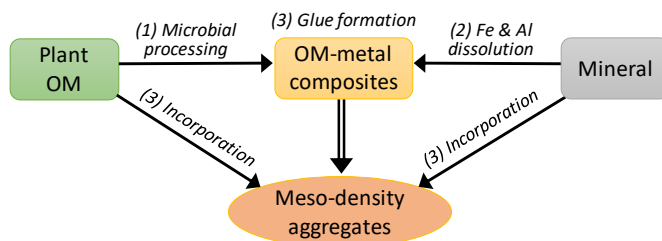
Figure 9: Conceptual illustration of meso-density aggregate formation. Three main processes are (1) microbial processing of plant-derived organic matter, (2) metal dissolution via chemical weathering, and (3) the formation of organo-metallic glue which promote meso-density microaggregate formation by incorporating some of POM and mineral.

940 **Tables**

Table 1. Sample source information and basic soil characteristics

Table 1. Sample source information and basic soil characteristics.

Sample ID	Site	Climate zone [a,b]	MAT °C	MAP mm yr⁻¹	Soil order [c]	Landuse [a]	Vegetation/Management	Horizon /depth (cm)	TOC mg g⁻¹	TN mg g⁻¹	Soil pH (H₂O)	Clay (%)
Andisols, allophanic												
A-1[d] / NIAES-NTa	Tsukuba, Japan	WTM	13.7	1300	Andisol	cropland	no-till with leaf compost	Ap/ 0-5	149	10	6.2	45-55
A-2[d] / NIAES-NTb								Ap/ 5-20	80.4	5.9	6.2	45-55
A-3[d] / NIAES-Till1							till + NPK	Ap/ 0-20	51.4	4.1	6.1	45-55
A-4[d] / NIAES-Till2							till (stump removed)	Ap/ 0-20	42.3	3.6	6.7	45-55
A-5 / NIAES-Bare							bare fallow	Ap/ 0-20	36.9	3.0	6.5	45-55
A-6 / TKY-NPK	Tokyo, Japan	WTM	14.7	1515	Andisol	cropland	till + NPK	Ap/ 0-14	46.5	3.9	4.1	27
A-7 / TKY-comp							till + NPK + compost	Ap/ 0-14	60.3	5.4	5.0	28
A-8 / YMS-NPK	Yamanashi, Japan	WTM	12.1	1137	Andisol	cropland	till + NPK	Ap/ 0-14	29.1	2.8	6.6	28
A-9 / YMS-straw							till + NPK + rice straw	Ap/ 0-14	35.5	3.2	6.7	28
A-10 / MtTKB-A	Tsukuba, Japan	WTM	|13.1	1438	Andisol	forest	secondary forest (mixed)	A/ 0-15	97.7	7.6	4.6	35-45
Andisols, non-allophanic												
N-1[e] / KWT-A1	Kawatabi, Japan	WTM	10.1	1460	Andisol	grassland	semi-managed	A1/ 0-25	105	6.7	4.6	23
N-2[e] / KWT-A2								A2/ 25-52	102	5.6	4.6	18
N-3[e] / KWT-2A3								2A3/ 52-100	98.3	4.9	4.9	25
N-4[e] / KWT-3Bw								3Bw/ 120-140	12.1	0.9	5.2	11
Spodosols												
S-1 / MBB-CN	Maine, USA	CTM	~5	1365	Spodosol	forest	conifer (red spruce)	Bhs/ 5-15	146	5.8	3.7	18-35
S-2 / MBB-DD						forest	mixed hardwood	Bhs/ 7-22	58.9	2.4	4.6	18-35
Crystalline mineralogy soils												
C-1 / NGK-straw	Aichi, Japan	WTM	14.9	1447	Inceptisol	cropland	rice paddy + manure	Ap/ 0-15	24.1	2.1	5.9	
C-2 / WKY-NPK	Wakayama, Japan	WTM	15.3	1286	Ultisol	cropland	till + NPK	Ap/ 0-16	9.8	1.0	5.8	15-25
C-3 / WKY-straw						cropland	till + NPK + manure	Ap/ 0-16	28.8	2.5	6.4	15-25
C-4 / MNG-A	NE Mongolia	CTD	ND	221	Mollisol	grassland	forest steppe	A1/ 0-10	24.2	2.5	6.3-7.2	15-25
C-5 / KIN-07S	Saba, Malaysia	TW	24.0	2392	Ultisol	forest	tropical (hill dipterocarp)	A/ 0-10	20.9	1.9	3.9	33-38
C-6 / KIN-17S	Saba, Malaysia	TM	19.0	2380	Inceptisol	forest	tropical (lower montane)	A/ 0-10	42.0	2.5	4.1	10-13
C-7 / KIN-27S	Saba, Malaysia	WTM	13.0	2256	Inceptisol	forest	tropical (upper montane)	A/ 0-10	125	8.4	3.9	6-15

[a] Based on 2006 IPCC Guidelines for National Greenhouse Gas Inventories. Vol. 4. Chapter 3: Consistent Representation of Lands.

[b] Climate zones. WTM: warm temperate moist, CTM: cool temperate moist, CTD: cool temperate dry, TW: tropical wet, and TM: tropical montane.

[c] Soil taxonomy, USDA, soil survey staff.

[d] Data from Wagai et al. (2018). A well-studied allophanic Andisol at the experimental field of NIAES/NARO, developed on andesitic and basaltic volcanic ashes.

[e] N1-N4: Kawatabi Andisol (Pacllic Mdanudand) is a typical, non-allophanic Andisol at Kawatabi Field Science Center of Tohoku University, Miyagi, Japan, located on a gentle slope of a fan in mountain valleys at 190 m elevation under native grassland (Sasa nipponica). Parent material is dacitic volcanic tephra with alluvium including smectitic sedimentary rock.

945 **Table 2. Recoveries of mass, C, N, and the metals dissolved by initial pyrophosphate (PP) and subsequent acid oxalate (OX) and dithionite-citrate (DC) extractions from the density fractions, expressed as percentage relative to the whole soil. Values show means (standard deviations) of all soils and separately for Andisols (allophanic and non-allophanic Andisols) and non-Andisols (Spodosols and crystalline mineral soils).**

Soil group	Mass	C	N	PP extr. Al+0.5Fe	OX extr. Al+0.5Fe	DC extr. Al+0.5Fe	Sum of PP, OX, and DC extractions		
							Al	Fe	Si
All soils (n=23)	99.8 (2.9)	97.5 (9.5)	95.6 (10.6)	104.6 (33.3)	98.8 (20.5)	86.4 (16.9)	88.8 (16.0)	94.4 (11.2)	93.6 (20.4)
Non-Andisols (n=9)	96.8 (2.1)	90.3 (8.9)	86.8 (8.9)	83.9 (12.0)	89.4 (12.5)	86.7 (15.5)	78.7 (15.0)	86.7 (12.0)	80.8 (9.3)
Andisols (n=14)	101.3 (1.9)	102.2 (6.7)	101.3 (7.4)	117.9 (36.0)	104.9 (22.7)	86.3 (18.4)	95.4 (13.4)	99.3 (7.5)	101.9 (21.5)

Figure A1
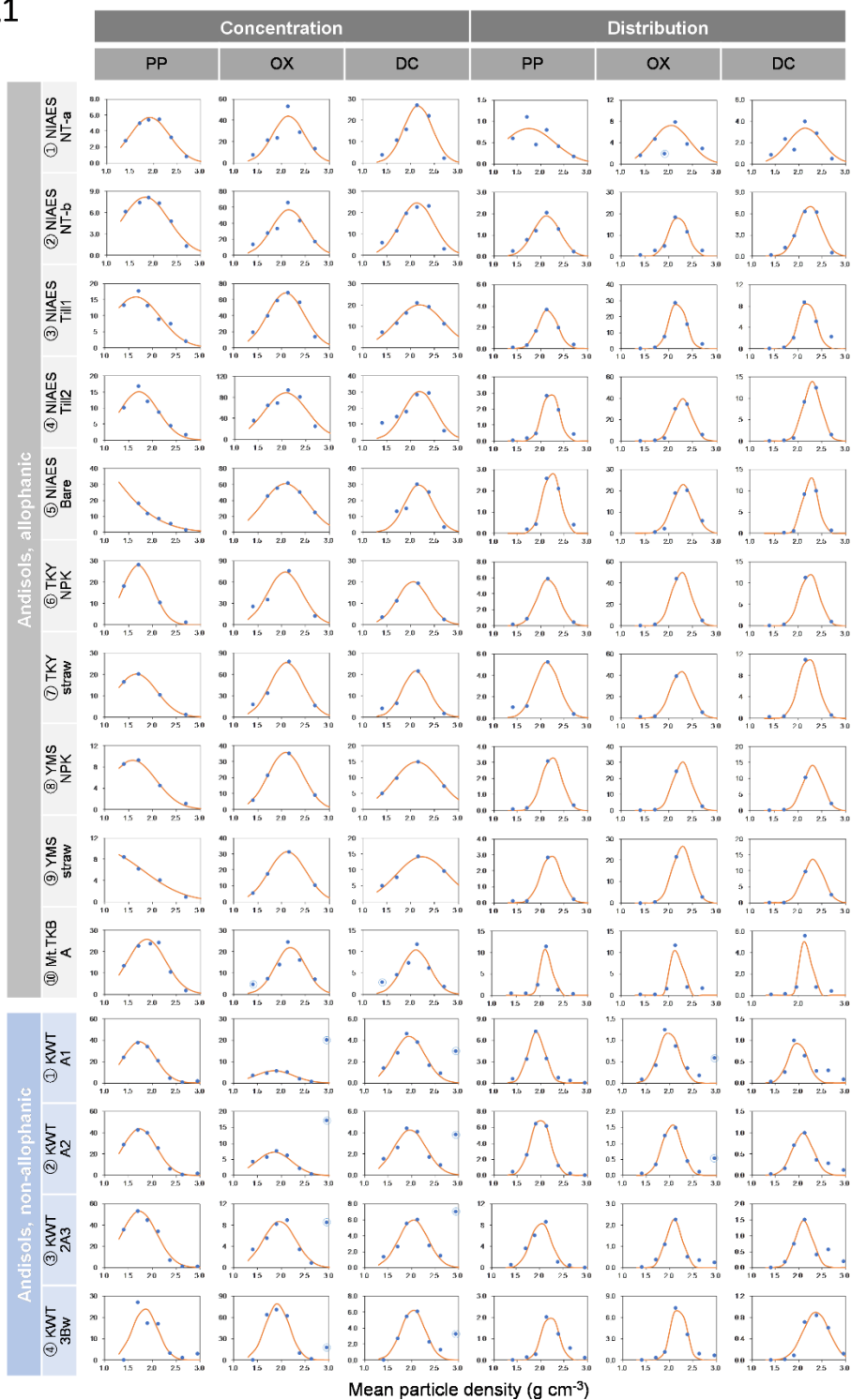
Mean particle density (g cm⁻³)
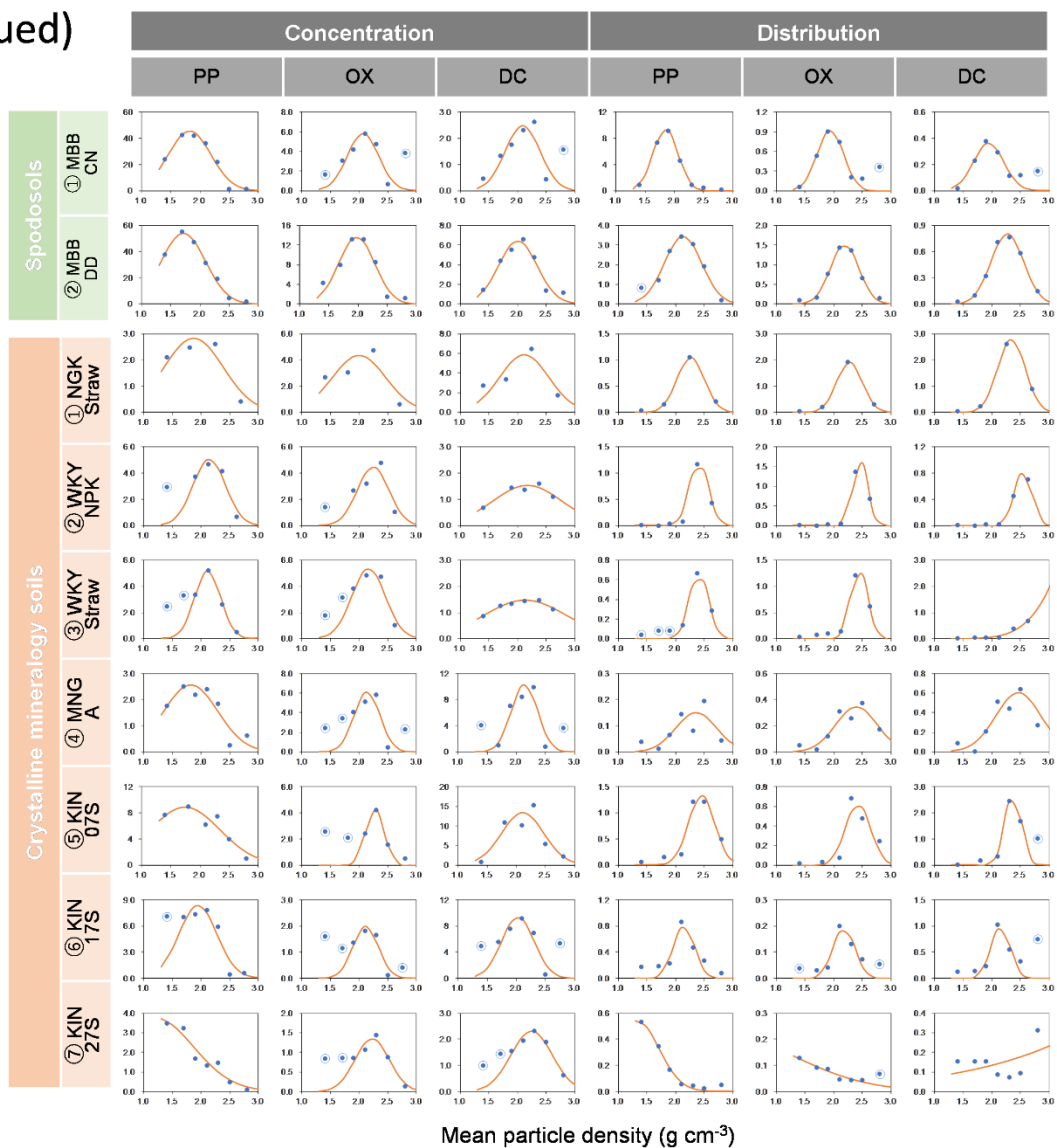
Figure A1: Extractable metal (Al+0.5Fe) against mean particle density for each soil sample. The metal concentrations (mg g^{-1} fraction) from pyrophosphate (PP), acid oxalate (OX), and dithionite-citrate (DC) extractions are shown in the left three panels. The distributions of PP, OX, DC-extractable metal phases (mg g^{-1} whole soil) are in the right three panels. Normal distribution curve fit is shown as line. The data points circled in blue were omitted from the fitting.

955
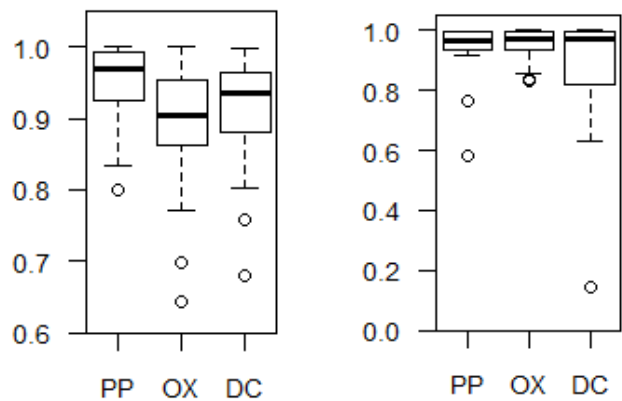
960 **Figure A2: Boxplot of r squared value for the normal distribution curve fitting of the extractable metal concentration (a) and distribution (b) against mean particle density. The fitting was done for each soil and each extraction as shown in Fig. A1.**
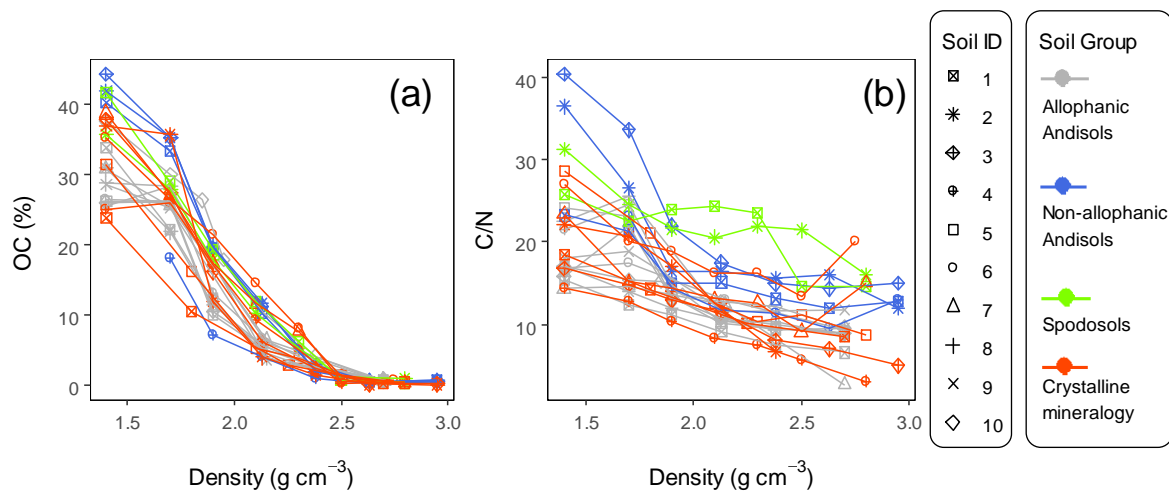
965 **Figure A3: Line graphs showing organic C concentration per fraction, as weight % (a) and C:N ratio (b) against soil particle density. Each line represents each soil sample which belongs to one of the four soil groups. Soil ID numbers, shown in different symbol shapes, correspond to Table 1.**
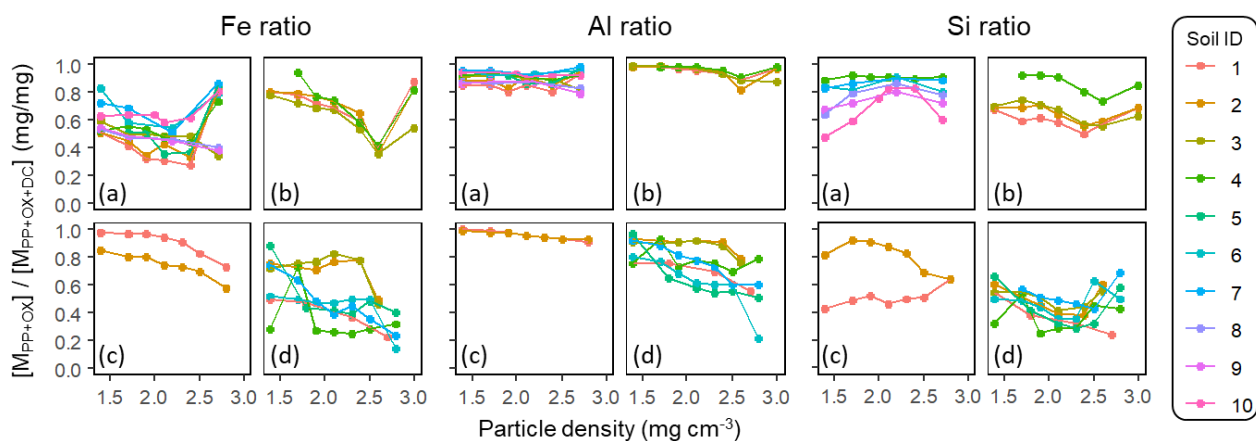
970

Figure A4: Proportion of total extractable Fe (left), Al (center), and Si (right panels) present as pyrophosphate- plus oxalate-extractable phases. This ratio obtained from each density fraction was shown along the density gradient for allophanic Andisols (a), non-allophanic Andisols (b), Spodosols (c), and crystalline mineralogy group (d). Each symbol represents individual soil sample ID in Table 1.

975
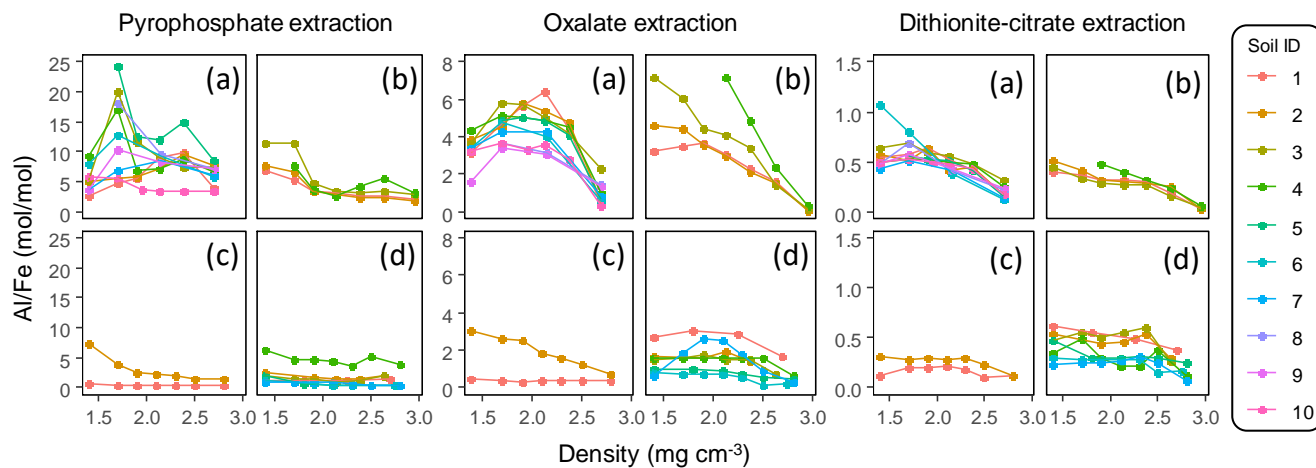
980

Figure A5: Molar Al-to-Fe ratio of each extractable phase from each density fraction along the density gradient. The ratio was shown for initial pyrophosphate (left four plots), subsequent acid oxalate (middle four plots), and final dithionite-citrate extractions (right four plots) were shown for Allophanic Andisols (a), non-allophanic Andisols (b), Spodosols (c), and crystalline mineralogy group (d). Each symbol represents individual soil sample ID in Table 1.

985
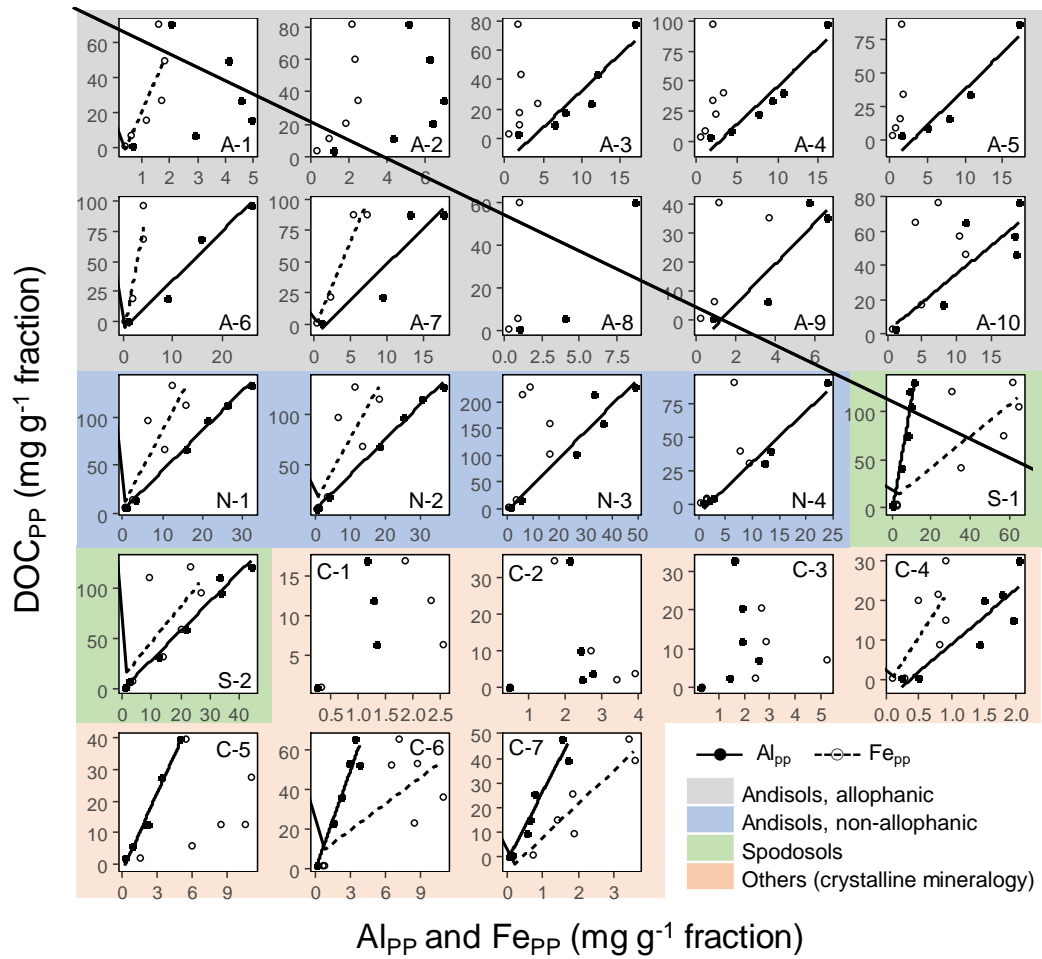
990 **Figure A6: Scattered plots of pyrophosphate-extractable Fe and Al against dissolved organic C concentration for each soil sample. Soil sample ID in each plot corresponds to that from Table 1. Solid lines represent significant linear regressions at p <0.1.**

995

1000
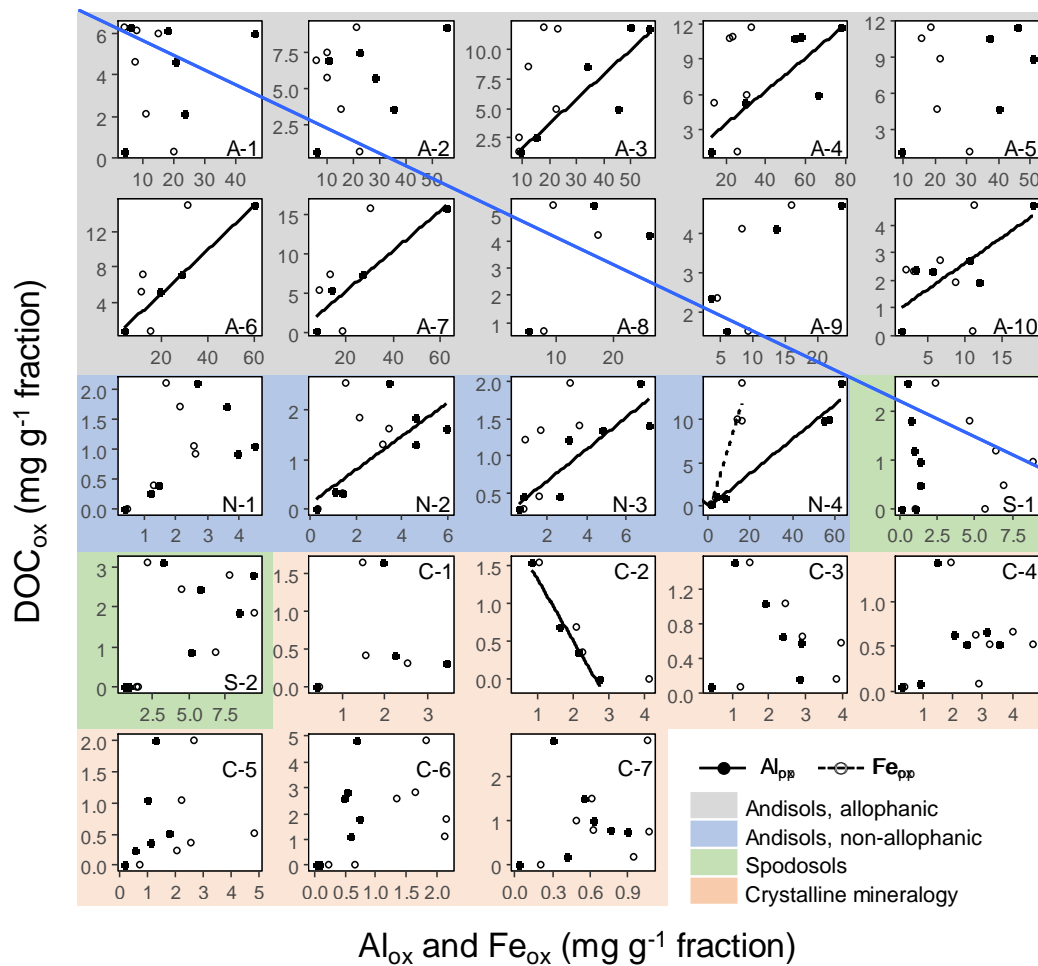
Figure A7: Scattered plots of acid-oxalate-extractable Fe and Al against dissolved organic C concentration for each soil sample. Soil sample ID in each plot corresponds to that from Table 1. Solid lines represent significant linear regressions at p <0.1.

1005

1010

1015
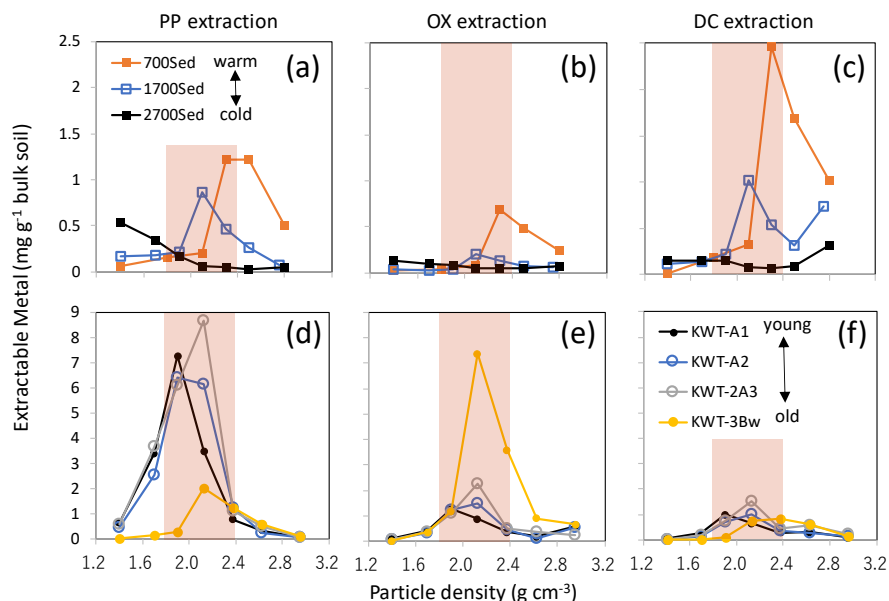
Figure A8: The distribution of the extractable metal phases (Al+0.5Fe) along the particle density gradient for two soil series. Upper three plots show PP- (a), OX- (b), and DC-extractable metals (c) for three A horizon soils under tropical forest along an elevation gradient from a weathered soil under warm climate at 700 m (sample ID: C5), moderately weathered soil at 1700 m (C6), and much less weathered soil at 2700 m (C7). The lower panels (d, e, f) showed surface and buried horizons of a non-allophanic Andisol profile (sample ID: N1-N4) that received multiple tephra deposits. Shaded zones show the meso-density range.

1020

Discussion associated with Fig. A8.

The relative balance of the three processes (OM supply and microbial processing, metal dissolution via weathering, and

1025 their binding/aggregation, Fig. 9) appear to control the nature of meso-density metal enrichment. Environmental gradients (e.g., climo- and chrono-sequences) give clear shifts in the balance of the three. Along a strong temperature gradient on a forested mountain slope, surface soils at higher altitudes experience slower rates of OM decay (thus higher OM accumulation) and mineral weathering than those at warmer lower-altitude soils. The majority of pedogenic metals in the 2700-m soil altitude (C-5) was present as PP-extractable phase and their distribution was peaked at <2.0 g cm^{-3} fractions whereas the 700-m altitude

1030 soil (C-7) held the metals mostly as DC- and PP-extractable phases that were mainly present at >2.2 g cm^{-3}, and the mid-altitude soil (C-6) showed the patterns in between them (Fig. A8a-c). Meso-density metal enrichment was strongest in the 700-m soil. This result can be explained by (1) higher microbial processing of OM as the forest productivity and thus OM supply to soil was the highest (Kitayama and Aiba, 2002;Wagai et al., 2008), and (2) higher degree of weathering under the warm moist climate regime (Wagai et al., 2009).

1035 Along with a volcanic soil profile experiencing up-building pedogenesis, we also observed the decline in metal$_{PP}$ and a concurrent increase in metal$_{OX}$ over pedogenic time (from upper to lower horizons), implying a shift in dominant metal phase from organo-metal complexes to short-range-order mineral. Concurrently, we found the increase in metal distribution from

low towards higher density (Fig. A8d-f). The top three horizons (A1, A2, and 2A3) were developed over the last ca 10 kyr based on key tephra (Hijiori Pumice) identified between 2A3 and 3Bw horizon, suggesting that the organo-metallic glue enriched in PP-extractable phase was replaced by that rich in OX-extractable phase over ca 10 kyrs under reduced OM input (buried) condition.

These results therefore suggest general patterns in the localization of specific metal phases and the mode of OM-metal association across scales as follows: (i) Al and Fe released by weathering preferentially bind to organic ligands to form organo-metallic complex in OM-rich environment (e.g., surface horizon esp. under cooler climate) and (ii), under the pedogenic condition where net organic supply to mineral surface is limited for a prolonged time (e.g., rapid decomposition under warm, wet condition and deeper horizons), polymerization of Fe and Al (and Si) is facilitated. The latter leads to the formation of short-range-order mineral which is further transformed to well-crystalline oxides over time. In other words, pedogenic reactions such as dynamics of mobile weathering products and secondary mineral formation occurring at a pedon scale (e.g., the depth-dependent framework, (Lawrence et al., 2015)) can be observed within bulk soils by the current approach combining sequential density fractionation with the extraction of operationally-defined metal phases.

References for A8

Kitayama, K., and Aiba, S. I.: Ecosystem structure and productivity of tropical rain forests along altitudinal gradients with contrasting soil phosphorus pools on Mount Kinabalu,Borneo, Journal of Ecology, 90, 37, 2002.

Lawrence, C. R., Harden, J. W., Xu, X., Schulz, M. S., and Trumbore, S. E.: Long-term controls on soil organic carbon with depth and time: A case study from the Cowlitz River Chronosequence, WA USA, Geoderma, 247–248, 73-87, http://dx.doi.org/10.1016/j.geoderma.2015.02.005, 2015.

Wagai, R., Mayer, L. M., Kitayarna, K., and Knicker, H.: Climate and parent material controls on organic matter storage in surface soils: A three-pool, density-separation approach, Geoderma, 147, 23-33, 10.1016/j.geoderma.2008.07.010, 2008.

Wagai, R., Mayer, L. M., and Kitayama, K.: Extent and nature of organic coverage of soil mineral surfaces assessed by a gas sorption approach, Geoderma, 149, 152-160, 10.1016/j.geoderma.2008.11.032, 2009.

Table A1. Concentrations of OC, N, and the elements extracted by pyrophosphate, acid-oxalate, and dithionite-citrate reagents in bulk and density fractions from each of 23 soil samples.

soil ID	mean density $g\ cm^{-3}$	low cutoff $g\ cm^{-3}$	high cutoff $g\ cm^{-3}$	mass fraction fraction	OC $mg\ g^{-1}$	N $mg\ g^{-1}$	C/N	Pyrophosphate-extractable (PP) $mg\ g^{-1}$ Al	Fe	Si	Mn	DOC	TDN	Acid-oxalate-extractable (OX) $mg\ g^{-1}$ Al	Fe	Si	Mn	TDN	Dithionite-extractable (DC) $mg\ g^{-1}$ Al	Fe	Si	Mn	PP-extr Al+0.5Fe $mg\ g^{-1}$	OX-extr Al+0.5Fe $mg\ g^{-1}$	DC-extr $mg\ g^{-1}$
A-1 / NIA-NTa	1.40		1.60	0.22	339	21.9	15.5	2.02	1.60	N.A.	0.29	70.21	6.64	5.76	3.81	3.05	0.13	0.41	1.40	5.28	3.52	0.07	2.82	7.66	4.04
	1.70	1.60	1.80	0.22	222	18.0	12.4	4.10	1.79	N.A.	0.39	49.41	2.89	17.69	7.82	9.70	0.28	0.50	3.87	13.84	5.39	0.07	4.99	21.60	10.80
	1.90	1.80	2.00	0.09	121	10.9	11.1	4.54	1.69	N.A.	0.34	26.57	2.03	20.08	7.43	10.29	0.25	0.42	6.09	19.72	5.35	0.16	5.39	23.80	15.95
	2.13	2.00	2.25	0.15	47	5.1	9.2	4.92	1.13	N.A.	0.18	15.16	1.26	46.02	14.87	27.46	0.48	0.66	9.08	36.33	7.18	0.25	5.48	53.45	27.25
	2.38	2.25	2.50	0.13	22	2.9	7.5	2.92	0.62	N.A.	0.11	7.09	0.79	23.33	10.90	13.42	0.37	0.28	6.31	31.63	4.71	0.20	3.23	28.79	22.12
	2.70	2.50		0.22	4.6	0.75	6.2	0.68	0.37	N.A.	0.03	0.93	0.23	3.72	19.75	2.88	0.17	0.04	0.33	4.05	1.16	0.04	0.86	13.59	2.35
	BULK				149	10.0	14.9	1.60	1.50	1.16	0.37	N.A.	N.A.	19.10	8.60	11.11	0.34	N.A.	3.60	15.10	4.29	0.10	2.35	23.40	11.15
A-2 / NIA-NTb	1.40		1.60	0.04	309	18.2	17.0	5.09	2.14	N.A.	0.49	81.68	3.36	10.73	5.82	5.65	0.23	0.41	2.11	7.70	3.54	0.06	6.16	13.64	5.96
	1.70	1.60	1.80	0.10	218	15.7	13.9	6.23	2.32	N.A.	0.48	59.74	3.13	22.55	10.27	12.37	0.35	0.54	3.78	15.36	4.17	0.08	7.39	27.68	11.46
	1.90	1.80	2.00	0.15	113	9.4	12.0	6.92	2.51	N.A.	0.33	34.28	2.42	28.25	10.09	13.96	0.37	0.48	7.45	24.28	4.76	0.21	8.17	33.29	19.59
	2.13	2.00	2.25	0.28	58	5.5	10.6	6.38	1.88	N.A.	0.17	20.89	1.60	55.42	21.35	32.73	0.57	0.89	6.51	32.09	3.62	0.15	7.32	66.09	22.55
	2.38	2.25	2.50	0.27	26	2.8	9.5	4.34	0.94	N.A.	0.11	11.45	0.85	35.51	15.31	19.24	0.56	0.39	7.07	32.41	4.09	0.23	4.81	43.17	23.27
	2.70	2.50		0.17	5.7	0.65	8.9	1.18	0.32	N.A.	0.04	3.59	0.28	6.19	22.26	4.10	0.25	0.07	0.43	5.45	0.72	0.04	1.34	17.32	3.15
	BULK				80	5.9	13.6	3.50	1.20	0.47	0.18	N.A.	N.A.	35.50	14.00	18.94	0.41	N.A.	5.60	26.60	3.49	0.18	4.10	42.50	18.90
A-3 / NIA-Till1	1.40		1.60	0.01	261	16.4	15.9	11.12	4.33	N.A.	0.22	24.21	1.63	15.13	8.59	7.15	0.24	0.16	2.73	8.93	2.23	0.06	13.29	19.43	7.19
	1.70	1.60	1.80	0.02	262	12.0	21.9	16.89	1.74	N.A.	0.12	77.64	2.94	33.66	11.96	15.96	0.50	0.39	4.58	13.92	1.98	0.09	17.75	39.64	11.54
	1.90	1.80	2.00	0.13	105	8.0	13.1	11.98	2.13	N.A.	0.13	43.58	2.58	49.65	17.97	24.84	0.68	0.91	5.87	20.47	2.48	0.10	13.04	58.63	16.10
	2.13	2.00	2.25	0.42	56	5.2	10.8	7.87	1.79	N.A.	0.07	18.26	1.29	56.84	23.30	28.73	0.80	1.09	7.28	27.14	2.74	0.13	8.77	68.49	20.85
	2.38	2.25	2.50	0.27	23	2.4	9.6	6.47	1.82	N.A.	0.09	9.65	0.71	45.47	22.47	24.79	0.90	0.53	6.02	26.21	2.61	0.13	7.38	56.70	19.12
	2.70	2.50		0.20	7.1	0.77	9.2	1.73	0.49	N.A.	0.04	3.04	0.34	9.46	8.66	4.73	0.37	0.15	2.59	17.38	1.17	0.10	1.97	13.79	11.28
	BULK				51	4.1	12.5	5.00	1.00	0.47	0.05	N.A.	N.A.	41.60	18.50	21.06	0.71	N.A.	6.30	25.50	2.57	0.14	5.50	50.85	19.05
A-4 / NIA-Till2	1.40		1.60	0.01	255	11.9	21.4	9.20	2.06	1.12	0.22	34.34	1.48	29.36	14.08	11.90	0.50	0.25	3.52	14.81	1.75	0.08	10.23	36.39	10.93
	1.70	1.60	1.80	0.01	283	11.5	24.6	16.04	1.95	1.14	0.11	97.47	3.34	54.35	22.12	21.54	0.92	0.44	5.03	19.80	1.94	0.12	17.02	65.41	14.93
	1.90	1.80	2.00	0.04	131	8.9	14.7	10.61	3.25	0.55	0.13	40.48	2.22	57.52	23.49	23.61	0.88	0.74	6.01	23.77	2.48	0.13	12.23	69.26	17.89
	2.13	2.00	2.25	0.32	65	6.3	10.3	7.68	2.26	0.15	0.08	22.65	1.20	77.76	32.86	33.41	1.07	1.14	9.33	38.75	3.44	0.24	8.81	94.19	28.70
	2.38	2.25	2.50	0.42	28	2.7	10.4	4.15	0.97	BD	0.05	8.94	0.48	66.27	30.44	29.41	1.35	0.58	9.30	40.52	3.44	0.25	4.63	81.49	29.55
	2.70	2.50		0.25	6.0	0.70	8.6	1.55	0.49	BD	0.02	3.32	N.A.	12.24	25.40	6.03	0.39	0.13	1.21	9.71	0.63	0.04	1.80	24.94	6.07
	BULK				42	3.6	11.8	3.81	1.27	0.56	0.08	13.33	1.04	53.38	29.82	23.44	0.95	N.A.	6.49	31.39	2.73	0.17	4.44	68.29	22.18
A-5 / NIA-Bare	1.40		1.60	0.01	262	10.9	24.1	N.A.	N.A.	N.A.	N.A.	NA	NA	N.A.	N.A.	N.A.	N.A.	NA	N.A.	N.A.	N.A.	N.A.			
	1.70	1.60	1.80	0.01	259	11.2	23.2	17.23	1.47	N.A.	0.10	86.04	3.21	37.22	15.85	18.00	0.46	0.46	4.69	17.20	2.02	0.10	17.96	45.14	13.29
	1.90	1.80	2.00	0.09	99	7.4	13.4	10.77	1.79	N.A.	0.12	33.66	2.23	45.90	18.75	23.08	0.53	0.86	4.96	19.77	2.23	0.10	11.66	55.28	14.85
	2.13	2.00	2.25	0.30	52	5.2	10.0	7.80	1.35	N.A.	0.10	16.00	1.40	50.96	21.58	26.30	0.50	0.88	9.85	40.69	4.19	0.31	8.47	61.75	30.19
	2.38	2.25	2.50	0.40	24	2.6	9.6	4.92	0.68	N.A.	0.02	9.07	0.70	40.39	20.32	20.87	0.80	0.49	7.08	35.90	2.89	0.19	5.26	50.55	25.03
	2.70	2.50		0.24	6.3	0.69	9.2	1.48	0.36	N.A.	0.02	3.49	0.26	30.94	5.25	5.25	0.44	0.12	0.43	5.53	0.33	0.04	1.67	24.99	3.20
	BULK				37	3.0	12.3	3.60	0.50	0.51	0.04	N.A.	N.A.	39.60	18.50	20.08	0.59	N.A.	5.80	30.10	2.40	0.15	3.85	48.85	20.85
A-6 / TKY-NPK	1.40		1.60	0.01	265	15.8	16.8	15.84	4.18	2.57	0.32	68.01	5.90	19.74	11.92	10.84	0.28	0.31	1.79	3.47	2.52	N.A.	17.93	25.70	3.53
	1.70	1.60	1.80	0.03	262	15.0	17.5	25.86	4.23	2.40	0.24	96.26	4.41	29.02	12.51	15.33	0.57	0.41	4.78	12.46	3.95	N.A.	27.98	35.28	11.01
	2.15	1.80	2.50	0.58	59	4.5	13.0	9.19	2.05	0.87	0.08	19.22	0.98	60.23	31.27	39.33	0.94	1.16	5.19	28.51	4.18	N.A.	10.21	75.87	19.44
	2.70	2.50		0.38	4.7	0.51	9.2	0.97	0.34	0.23	0.01	0.46	BD	4.27	15.56	4.14	0.17	0.08	0.24	4.16	1.08	N.A.	1.14	12.05	2.32
	BULK				46	3.9	11.8	8.09	1.69	0.79	0.10	16.52	0.99	42.97	25.57	28.30	0.75	0.87	3.03	19.46	2.79	N.A.	8.94	55.75	12.76
A-7 / TKY-Comp	1.40		1.60	0.06	307	21.5	14.3	13.00	7.15	2.42	0.30	87.29	6.93	13.82	8.37	8.58	0.11	0.38	1.21	5.96	2.43	N.A.	16.58	18.01	4.19
	1.70	1.60	1.80	0.06	256	17.5	14.6	17.60	5.35	2.08	0.37	87.77	6.15	27.27	13.34	16.56	0.53	0.51	2.15	8.83	3.15	N.A.	20.27	33.94	6.57
	2.15	1.80	2.50	0.51	63	5.1	12.4	9.28	2.28	0.94	0.15	21.52	1.13	63.00	30.44	40.34	1.01	1.28	6.08	31.06	4.95	N.A.	10.42	78.26	21.61
	2.70	2.50		0.35	5.7	2.1	2.8	1.01	0.34	0.24	0.02	0.50	BD	6.91	18.23	6.14	0.18	0.11	0.21	3.00	0.89	N.A.	1.18	16.02	1.71
	BULK				60	5.4	11.2	6.98	1.88	0.81	0.15	20.15	1.31	36.91	22.47	24.93	0.64	0.82	2.79	18.01	2.87	N.A.	7.92	48.15	11.80
A-8 / YMS-NPK	1.40		1.60	0.01	288	12.8	22.5	N.A.*	N.A.*	N.A.*	N.A.*	N.A.*	N.A.*	N.A.*	N.A.*	N.A.*	N.A.*	N.A.*	N.A.*	N.A.*	N.A.*	N.A.*	N.A.*	N.A.*	N.A.*
	1.70	1.60	1.80	0.01	283	11.1	25.6	8.70	1.00	0.43	0.15	59.94	2.52	16.57	9.37	6.04	0.43	0.21	3.94	11.78	1.76	0.00	9.20	21.25	9.83
	2.15	1.80	2.50	0.70	37	3.5	10.5	4.01	0.87	0.70	0.05	5.68	0.39	26.40	17.37	13.57	0.83	0.40	4.29	21.24	2.26	0.13	4.45	35.09	14.90
	2.70	2.50		0.29	7.1	0.77	9.3	0.96	0.28	0.27	0.01	0.72	BD	5.18	7.72	2.33	0.33	0.08	1.32	12.08	0.75	0.13	1.10	9.05	7.36
	BULK				29	2.8		2.54	0.54	0.51	0.05	4.90	0.32	21.26	13.78	9.03	N.A.	N.A.	3.80	19.93	1.82	N.A.	2.80	28.16	13.77
A-9 / YMS-Straw	1.40		1.60	0.02	286	15.9	17.9	6.65	3.72	2.83	0.18	35.44	1.62	3.39	4.48	1.30	0.04	0.13	1.59	6.98	2.03	N.A.	8.51	5.63	5.08
	1.70	1.60	1.80	0.02	252	13.4	18.8	5.69	1.13	1.39	0.34	40.42	1.34	13.47	8.20	5.27	0.39	0.22	2.74	10.00	2.67	N.A.	6.25	17.57	7.74
	2.15	1.80	2.50	0.69	35	3.0	11.7	3.65	0.93	0.88	0.11	6.49	0.44	23.49	15.81	10.21	0.78	0.41	4.16	20.37	2.79	N.A.	4.11	31.40	14.34
	2.70	2.50		0.27	7.0	0.65	10.8	0.83	0.24	0.30	0.02	0.45	BD	5.97	9.14	2.58	0.38	0.13	1.81	15.76	1.14	N.A.	0.94	10.53	9.69
	BULK				35	3.2	11.0	2.26	0.56	0.67	0.10	6.68	0.42	19.09	12.95	8.36	0.60	0.37	3.83	19.94	2.51	N.A.	2.54	25.56	13.80
A-10 / MTT-A	1.40		1.60	0.03	376	22.2	17.0	11.38	4.01	1.15	0.44	65.48	4.17	3.42	2.21	0.96	0.08	0.14	0.91	3.82	2.35	0.03	13.38	4.53	2.82
	1.70	1.60	1.80	0.02	300	19.5	15.4	19.08	7.27	1.63	0.45	76.58	4.93	5.74	3.25	1.72	0.13	0.15	1.54	6.15	2.39	0.04	22.71	7.37	4.62
	1.85	1.80	1.90	0.07	263	17.3	15.2	N.A.	N.A.	N.A.	N.A.	N.A.	N.A.	N.A.	N.A.	N.A.	N.A.	N.A.	N.A.	N.A.	N.A.	N.A.	N.A.	N.A.	N.A.
	1.95	1.90	2.00	0.11	178	13.2	13.5	18.44	10.53	2.28	0.40	57.42	3.63	10.66	6.66	3.57	0.30	0.20	2.37	10.02	1.95	0.06	23.71	13.99	7.37
	2.13	2.00	2.25	0.47	105	8.2	12.7	18.53	11.39	2.18	0.40	46.23	2.91	19.06	11.13	6.34	0.67	0.37	3.68	16.19	1.85	0.12	24.23	24.63	11.78
	2.38	2.25	2.50	0.12	40	3.3	12.3	8.13	4.92	0.92	0.27	17.27	1.05	11.75	8.81	4.16	0.82	0.16	1.81	8.65	1.08	0.07	10.59	16.15	6.14
	2.70	2.50		0.23	4.8	0.46	10.3	1.30	0.81	0.03	0.05	2.62	0.15	1.64	11.02	0.63	0.12	0.02	0.25	3.03	0.44	0.02	1.71	7.15	1.76
	BULK				98	7.6	13.7	12.64	7.52	1.46	0.36	37.08	2.43	12.87	7.72	4.15	0.53	0.22	2.44	10.30	1.44	N.A.	16.40	16.13	7.59
N-1 / KWT-A1	1.40		1.60	0.03	404	17.4	23.2	21.16	6.33	2.84	0.28	97.27	4.23	2.68	1.70	0.48	0.06	0.09	0.40	2.05	1.63	N.A.	24.32	3.53	1.43
	1.70	1.60	1.80	0.09	333	15.6	21.4	31.99	12.29	2.22	0.31	134.07	6.23	3.61	2.15	0.68	0.17	0.08	0.74	4.20	2.05	0.03	38.14	4.68	2.84
	1.90	1.80	2.00	0.21	196	13.1	14.9	25.97	15.97	2.60	0.34	112.80	6.34	4.53	2.59	1.03	0.27	0.07	1.08	7.12	2.33	0.05	33.96	5.83	4.64
	2.13	2.00	2.25	0.17	101	6.7	15.1	15.83	10.40	1.85	0.40	66.72	3.51	3.95	2.64	0.94	0.50	0.06	0.89	5.95	2.04	0.04	21.03	5.27	3.87
	2.38	2.25	2.50	0.17	20	1.5	13.3	3.26	2.55	0.64	0.19	14.48	0.56	1.44	1.29	0.39	0.38	0.03	0.38	2.62	1.07	0.02	4.53	2.09	1.69
	2.63	2.50	2.75	0.12	4.8	0.43	11.2	0.72	0.61	0.34	0.03	5.52	N.A.	0.34	0.44	0.10	0.05	BD	0.14	1.56	0.34	0.01	1.03	0.55	0.92
	2.95	2.75		0.03	6.4	0.52	12.3	1.08	1.10	0.41	0.09	6.80	N.A.	1.21	37.98	0.33	0.32	0.02	0.07	5.89	0.34	0.05	1.63	20.20	3.01
	BULK				105	6.7	15.7	11.39	7.90	0.96	N.A.	N.A.	N.A.	1.73	0.99	0.26	N.A.	N.A.	1.38	5.00	1.81	N.A.	15.35	2.22	3.88
N-2 / KWT-A2	1.40		1.60	0.02	419	11.5	36.3	25.28	6.81	1.19	0.15	97.92	3.34	3.45	1.55	0.33	0.08	0.07	0.50	2.06	0.71	N.A.	28.69	4.22	1.53
	1.70	1.60	1.80	0.06	353	13.3	26.6	36.55	11.50	2.01	0.14	127.71	4.48	4.59	2.15	0.69	0.17	0.07	0.73	3.73	1.23	N.A.	42.30	5.66	2.60
	1.90	1.80	2.00	0.16	198	12.1	16.4	30.44	18.46	2.80	0.19	115.83	5.29	5.97	3.42	1.38	0.28	0.10	1.02	6.72	1.73	N.A.	39.67	7.68	4.38
	2.13	2.00	2.25	0.24	116	7.1	16.4	18.43	13.79	2.24	0.40	68.67	2.91	4.56	3.16	1.07	0.46	0.02	0.92	6.35	1.74	N.A.	25.33	6.14	4.09
	2.38	2.25	2.50	0.21	19	1.2	15.2	4.22	3.60	0.82	0.10	18.70	0.60	1.43	1.40	0.38	0.25	0.02	0.37	2.69	0.98	N.A.	6.01	2.13	1.72
	2.63	2.50	2.75	0.29	4.8	0.35	13.6	0.59	0.51	0.28	0.01	6.74	BD	0.23	0.32	0.07	0.02	BD	0.19	1.55	0.25	N.A.	0.85	0.39	0.97
	2.95	2.75		0.03	6.0	0.46	13.1	0.96	1.05	0.36	0.04	6.78	N.A.	1.04	32.29	0.31	0.24	0.03	0.08	7.52	0.31	N.A.	1.49	17.18	3.84
	BULK				102	5.6	20.1	18.67	10.44	1.42	N.A.	N.A.	N.A.	3.57	1.35	0.71	N.A.	N.A.	1.59	5.72	1.30	N.A.	23.89	4.24	4.44
N-3 / KWT-2A3	1.40		1.60	0.02	443	11.0	40.2	32.89	6.00	0.99	0.14	212.94	4.69	3.06	0.88	0.23	0.10	0.03	0.43	1.98	0.55	N.A.	35.89	3.49	1.42
	1.70	1.60	1.80	0.07	353	10.5	33.7	48.76	8.89	2.21	0.15	228.72	6.89	4.77	1.64	0.79	0.25	0.04	0.64	4.09	1.02	N.A.	53.21	5.59	2.69
	1.90	1.80	2.00	0.14	195	8.9	21.8	36.84	16.12	2.97	0.31	158.73	6.37	6.66	3.14	1.42	0.50	0.09	1.19	8.81	1.85	N.A.	44.89	8.23	5.60
	2.13	2.00	2.25	0.25	112	6.4	17.6	26.20	16.20	2.63	0.32	102.53	4.60	7.17	3.61	1.64	0.65	0.08	1.21	9.64	2.05	N.A.	34.30	8.98	6.03
	2.38	2.25	2.50	0.37	27	1.8	15.1	5.56	3.58	0.92	0.17	15.13	0.51	2.63	1.61	0.63	0.59	0.03	0.57	4.48	1.16	N.A.	7.35	3.44	2.81
	2.63	2.50	2.75	0.37	4.3	0.31	14.1	1.02	0.65	0.30	0.04	2.24	BD	0.55	0.82	0.12	0.23	0.02	0.20	2.72	0.34	N.A.	1.35	0.96	1.55
	2.95	2.75		0.03	4.5	0.30	15.3	1.05	0.78	0.32	0.05	2.60	BD	0.84	15.48	0.26	0.33	0.03	0.27	13.56	0.35	N.A.	1.44	8.58	7.05
	BULK				98	4.9	22.2	20.19	8.31	1.31	N.A.	N.A.	N.A.	6.13	1.89	1.41	N.A.	N.A.	1.85	5.96	1.40	N.A.	24.38	7.07	4.83
N-4 / KWT-3Bw	1.40		1.60	0.00	N.A.	N.A.	N.A.	N.A.	N.A.	N.A.	N.A.	N.A.	N.A.	N.A.	N.A.	N.A.	N.A.	N.A.	N.A.	N.A.	N.A.	N.A.	N.A.	N.A.	N.A.
	1.70	1.60	1.80	0.01	181	7.8	23.1	23.97	6.48	1.49	0.06	91.14	4.35	56.80	13.73	23.49	0.61	0.43	2.07	1.34	2.14	0.04	27.21	63.66	2.74
	1.90	1.80	2.00	0.02	71	4.9	14.3	13.35	7.80	1.19	0.08	39.38	1.73	62.68	16.06	31.39	0.63	0.98	1.72	7.50	2.72	N.A.	17.25	70.71	5.46
	2.13	2.00	2.25	0.12	39	3.3	11.7	12.38	9.57	0.82	0.07	29.80	1.33	54.78	15.71	26.68	0.55	0.83	1.69	8.83	2.93	N.A.	17.16	62.64	6.11
	2.38	2.25	2.50	0.36	9.0	0.75	11.9	2.70	1.38	0.48	0.01	3.80	BD	8.08	3.46	3.70	0.16	0.09	0.53	3.63	1.06	N.A.	3.39	9.81	2.30
	2.63	2.50	2.75	0.48	1.9	0.15	12.2	0.98	0.36	0.34	0.01	0.96	BD	1.29	1.12	0.60	0.09	0.03	0.24	2.09	0.36	N.A.	1.16	1.85	1.28
	2.95	2.75		0.04	3.9	0.29	13.1	2.16	1.50	0.50	0.03	2.94	0.22	4.49	26.59	2.13	0.40	0.08	0.17	6.26	0.47	N.A.	2.91	17.78	3.30
	BULK				12	0.93	13.1	5.49	2.14	0.65	0.01	0.97	0.74	11.31	4.33	2.95	0.19	N.A.	0.30	0.82	0.47	0.02	6.56	13.47	0.71

1075

Sample																									
S-1 / MBB-CN	1.40		1.60	0.04	418	16.2	25.9	8.99	30.29	0.73	24.14	121.29	3.66	0.52	2.38	0.08	1.71	0.10	0.05	0.85	1.08	0.47	24.14	1.71	0.47
	1.70	1.60	1.80	0.17	289	12.9	22.4	11.43	62.17	0.52	42.51	131.37	3.18	0.74	4.66	0.12	3.07	0.08	0.21	2.24	0.68	1.34	42.51	3.07	1.34
	1.90	1.80	2.00	0.22	193	8.1	23.9	9.88	65.06	0.37	42.41	104.88	2.40	0.98	6.45	0.19	4.20	0.05	0.28	2.95	0.53	1.76	42.41	4.20	1.76
	2.10	2.00	2.20	0.13	119	4.9	24.6	7.81	57.00	0.27	36.31	74.52	1.34	1.42	8.87	0.30	5.86	0.04	0.39	3.86	0.68	2.33	36.31	5.86	2.33
	2.30	2.20	2.40	0.04	61	2.6	23.7	4.58	35.28	0.24	22.21	40.66	0.65	1.35	6.91	0.52	4.81	0.02	0.40	4.50	0.78	2.65	22.21	4.81	2.65
	2.50	2.40	2.60	0.27	5.8	0.35	16.5	0.35	2.73	0.14	1.71	3.18	BD	0.19	1.02	0.12	0.70	BD	0.04	0.81	0.26	0.45	1.71	0.70	0.45
	2.80	2.60		0.10	2.9	0.20	14.5	0.50	2.23	0.39	1.61	2.17	BD	1.03	5.65	0.84	3.85	BD	0.16	2.86	0.70	1.59	1.61	3.85	1.59
	BULK				146	5.8	25.0	6.94	35.91	0.20	24.90	68.78	1.34	1.17	4.76	0.49	3.55	0.03	0.24	2.36	0.67	1.42	24.90	3.55	1.42
S-2 / MBB-DD	1.40		1.60	0.02	359	11.5	31.2	33.23	9.39	1.43	37.92	109.81	2.42	3.25	2.19	0.31	4.35	0.10	0.33	2.17	0.39	1.41	37.92	4.35	1.41
	1.70	1.60	1.80	0.02	278	11.4	24.3	43.76	23.34	3.94	55.43	120.78	3.24	5.75	4.53	1.55	8.02	0.10	0.94	6.94	0.52	4.41	55.43	8.02	4.41
	1.90	1.80	2.00	0.06	179	8.3	21.6	33.84	26.64	2.77	47.16	95.09	2.53	9.34	7.81	2.88	13.25	0.13	1.25	8.58	0.61	5.54	47.16	13.25	5.54
	2.10	2.00	2.20	0.11	103	5.0	20.5	21.51	20.40	1.79	31.71	58.85	1.65	8.48	9.54	2.55	13.25	0.09	1.37	10.44	0.67	6.58	31.71	13.25	6.58
	2.30	2.20	2.40	0.16	53	2.4	22.0	12.17	13.74	1.27	19.04	32.08	0.63	5.13	6.85	1.52	8.56	0.04	1.04	7.49	0.58	4.79	19.04	8.56	4.79
	2.50	2.40	2.60	0.43	11	0.54	19.6	2.61	3.59	0.40	4.41	7.19	BD	0.82	1.43	0.26	1.53	BD	0.24	2.22	0.30	1.36	4.41	1.53	1.36
	2.80	2.60		0.12	8.0	0.45	17.8	0.91	1.33	0.24	1.58	2.05	BD	0.52	1.47	0.24	1.25	BD	0.11	2.07	0.28	1.15	1.58	1.25	1.15
	BULK			0.92	59	2.4	24.1	11.25	10.82	1.21	16.66	30.43	0.67	2.76	3.10	0.77	4.31	0.02	0.57	4.76	0.43	2.95	16.66	4.31	2.95
C-1 / NGK-Manur	1.40		1.60	0.01	238	12.9	18.4	1.15	1.86	2.34	0.12	17.05	1.28	1.93	1.48	0.67	0.02	0.09	1.01	3.42	2.51	0.01	2.08	2.67	2.72
	1.80	1.60	2.00	0.06	104	7.3	14.3	1.28	2.35	0.95	0.04	11.87	0.85	2.24	1.55	0.52	0.02	0.03	1.15	4.33	2.43	0.01	2.46	3.02	3.32
	2.25	2.00	2.50	0.40	28	2.8	10.1	1.32	2.56	0.48	0.02	6.26	0.56	3.47	2.54	0.62	0.03	0.03	2.08	8.73	2.34	0.01	2.60	4.74	6.45
	2.70	2.50		0.51	1.7	0.17	10.1	0.23	0.32	BD	0.02	0.87	BD	0.35	0.43	0.10	0.00	BD	0.46	2.52	0.33	BD	0.39	0.57	1.72
	BULK				24	2.1	11.4	0.67	1.46	0.22	0.02	4.09	0.31	1.72	1.26	0.32	0.02	0.03	1.14	4.92	1.39	0.01	1.40	2.35	3.59
C-2 / WKY-NPK	1.40		1.60	0.005	369	16.7	22.1	2.12	1.68	1.35	0.19	34.48	2.51	0.86	1.05	0.37	0.02	0.07	0.23	0.89	1.12	0.00	2.96	1.39	0.67
	1.70	1.60	1.80	0.003	356	17.2	20.7	N.A.	N.A.	N.A.	N.A.	N.A.	N.A.	N.A.	N.A.	N.A.	N.A.	N.A.	N.A.	N.A.	N.A.	N.A.	N.A.	N.A.	N.A.
	1.90	1.80	2.00	0.01	119	7.0	17.1	2.39	2.71	1.03	0.30	10.03	1.09	1.62	2.10	0.51	0.05	0.04	0.43	2.04	1.87	0.01	3.75	2.67	1.45
	2.13	2.00	2.25	0.02	39	3.3	11.9	2.73	3.90	0.70	0.43	3.67	0.91	2.11	2.24	0.74	0.21	0.03	0.42	1.91	2.31	0.02	4.67	3.24	1.37
	2.38	2.25	2.50	0.28	14	2.1	6.7	2.43	3.42	0.35	0.33	1.86	0.30	2.75	4.12	0.61	0.43	BD	0.55	2.12	1.58	0.04	4.14	4.81	1.61
	2.63	2.50	2.75	0.64	0.36	0.03	10.7	0.45	0.48	0.38	0.09	BD	0.48	1.16	0.29	0.22	BD	0.25	1.71	0.45	0.02	0.69	1.06	1.10	
	2.95	2.75		0.02	0.29	0.03	10.7	N.A.	N.A.	N.A.	N.A.	N.A.	N.A.	N.A.	N.A.	N.A.	N.A.	N.A.	N.A.	N.A.	N.A.	N.A.	N.A.	N.A.	N.A.
	BULK				9.8	1.0	9.4	1.29	1.68	0.45	0.30	1.96	0.30	1.39	2.17	0.46	0.17	0.30	1.96	1.01	0.02	2.13	2.47	1.32	
C-3 / WKY-Straw	1.40		1.60	0.02	379	22.6	16.8	1.61	1.66	1.07	0.43	32.94	3.08	1.06	1.46	0.39	0.05	0.09	0.27	1.19	1.26	0.01	2.44	1.79	0.87
	1.70	1.60	1.80	0.02	274	18.5	14.8	1.92	2.71	1.10	0.85	20.67	1.95	1.89	2.46	0.80	0.13	0.07	0.44	1.65	1.57	0.03	3.28	3.12	1.27
	1.90	1.80	2.00	0.02	161	12.5	12.9	1.88	2.89	1.05	0.85	11.75	1.41	2.38	2.89	0.96	0.14	0.05	0.44	1.78	1.98	0.03	3.33	3.83	1.33
	2.13	2.00	2.25	0.03	61	5.3	11.5	2.58	5.25	0.72	0.62	6.96	0.94	2.87	3.96	0.98	0.15	0.05	0.50	1.90	2.36	0.04	5.20	4.85	1.45
	2.38	2.25	2.50	0.25	22	2.8	7.9	1.40	2.42	0.51	0.41	2.32	0.18	2.81	3.84	0.83	0.30	0.02	0.53	1.85	1.76	0.06	2.61	4.73	1.46
	2.63	2.50	2.75	0.60	0.66	0.06	10.3	0.30	0.33	0.27	0.10	0.00	BD	0.41	1.21	0.28	0.23	0.01	0.23	1.80	0.45	0.03	0.47	1.02	1.13
	2.95	2.75		0.02	0.53	0.05	10.3	N.A.	N.A.	N.A.	N.A.	N.A.	N.A.	N.A.	N.A.	N.A.	N.A.	N.A.	N.A.	N.A.	N.A.	N.A.	N.A.	N.A.	N.A.
	BULK				29	2.5	11.7	1.06	1.97	0.61	0.44	2.35	0.53	1.41	2.77	0.59	0.12	0.02	0.39	2.47	1.14	0.04	2.04	2.80	1.63
C-4 / MNG-A	1.40		1.60	0.02	250	17.5	14.3	1.52	0.50	0.96	0.18	20.10	1.31	1.49	1.92	0.28	0.13	0.10	1.01	6.21	2.68	0.04	1.78	2.44	4.11
	1.70	1.60	1.80	0.01	261	20.5	12.7	2.06	0.92	1.35	0.25	30.00	1.89	2.06	2.77	0.68	0.22	0.05	0.32	1.37	1.84	0.02	2.52	3.45	1.01
	1.90	1.80	2.00	0.03	172	16.6	10.3	1.80	0.79	0.82	0.25	21.48	1.37	2.45	3.23	0.48	0.30	0.05	1.60	10.97	3.95	0.07	2.19	4.07	7.08
	2.10	2.00	2.20	0.06	92	11.0	8.3	1.96	0.91	0.80	0.16	14.96	0.99	3.11	4.02	0.62	0.34	0.04	1.49	13.96	3.64	0.04	2.41	5.12	8.47
	2.30	2.20	2.40	0.04	49	6.6	7.5	1.44	0.83	0.75	0.14	8.83	0.49	3.54	4.69	0.87	0.43	0.07	1.67	16.58	3.98	0.07	1.85	5.88	9.96
	2.50	2.40	2.60	0.74	1.7	0.34	4.9	0.22	0.09	0.21	0.02	0.39	BD	0.31	0.40	0.15	0.04	0.01	0.23	1.27	0.45	0.13	0.27	0.51	0.87
	2.80	2.60		0.07	2.8	0.89	3.1	0.49	0.27	0.19	0.03	0.66	BD	0.91	2.88	0.46	0.10	0.02	0.38	6.67	0.87	0.07	0.62	2.35	3.72
	BULK				24	2.5	9.7	0.49	0.25	0.44	N.A.	N.A.	N.A.	1.09	1.22	0.31	N.A.	0.56	4.52	1.30	N.A.	0.62	1.70	2.82	
C-5 / KIN-07S	1.40		1.60	0.01	315	11.0	28.5	4.93	5.46	1.17	0.02	39.47	2.14	1.26	2.65	0.37	BD	0.07	0.25	1.09	0.79	0.00	7.66	2.59	0.79
	1.80	1.60	2.00	0.02	162	7.7	20.9	3.46	10.96	0.67	0.01	27.58	1.01	0.99	2.20	0.17	BD	0.05	2.40	17.00	1.18	0.01	8.94	2.39	10.90
	2.10	2.00	2.20	0.03	51	4.1	12.5	1.97	8.42	0.53	0.01	12.53	0.70	1.12	2.54	0.19	BD	0.03	2.28	15.78	1.54	0.01	6.18	2.39	10.17
	2.30	2.20	2.40	0.16	37	3.6	10.3	2.29	10.43	0.21	0.01	12.40	0.57	1.78	4.87	0.19	BD	0.05	3.49	23.48	1.03	0.01	7.50	4.22	15.23
	2.50	2.40	2.60	0.31	12	1.1	10.8	1.00	5.92	0.14	BD	5.85	0.38	0.53	2.05	0.06	BD	0.02	1.24	8.48	0.41	0.01	3.95	1.56	5.48
	2.80	2.60		0.47	2.6	0.32	8.3	0.27	1.56	0.14	BD	1.99	BD	0.15	0.73	0.02	BD	BD	0.41	3.48	0.12	BD	1.05	0.51	2.15
	BULK				21	1.9	11.1	1.14	3.64	0.12	BD	1.70	0.58	0.79	2.13	0.08	BD	0.06	1.53	10.75	0.51	BD	2.96	1.86	6.91
C-6 / KIN-17S	1.40		1.60	0.02	353	13.1	26.9	3.78	6.57	0.52	0.01	52.69	2.32	0.69	1.82	0.08	BD	0.18	1.10	7.65	0.62	BD	7.06	1.60	4.93
	1.70	1.60	1.80	0.03	265	13.2	20.1	3.43	7.15	0.75	0.01	65.63	2.86	0.47	1.35	0.09	BD	0.13	1.19	8.59	0.91	BD	7.00	1.15	5.49
	1.90	1.80	2.00	0.03	214	11.4	18.8	2.92	8.81	0.75	0.01	53.72	2.73	0.54	1.64	0.11	BD	0.15	1.60	11.85	1.10	BD	7.33	1.36	7.53
	2.10	2.00	2.20	0.11	144	8.9	16.2	2.27	11.00	0.62	BD	36.69	1.96	0.72	2.17	0.15	BD	0.11	1.93	14.49	1.40	BD	7.77	1.80	9.18
	2.30	2.20	2.40	0.08	81	5.0	16.2	1.61	8.55	0.42	BD	23.24	1.18	0.58	2.14	0.09	BD	0.07	1.46	10.89	0.95	BD	5.88	1.65	6.90
	2.50	2.40	2.60	0.59	4.0	0.30	13.3	0.09	0.70	0.11	BD	1.91	BD	0.01	0.22	0.01	BD	BD	0.07	0.94	0.07	BD	0.44	0.12	0.54
	2.75	2.60		0.14	6.0	0.30	20.0	0.13	0.82	0.10	BD	1.95	BD	0.07	0.65	0.02	BD	BD	0.75	9.21	0.12	BD	0.54	0.39	5.35
	BULK				42	2.5	16.8	1.17	3.65	0.12	0.01	1.73	0.58	0.27	0.86	0.02	BD	0.02	0.07	0.59	0.17	BD	3.00	0.70	0.36
C-7 / KIN-27S	1.40		1.60	0.15	388	16.6	23.4	1.69	3.60	1.43	0.03	39.15	2.00	0.31	1.06	0.13	BD	0.12	1.65	0.59	BD	3.49	0.84	1.01	
	1.70	1.60	1.80	0.11	271	17.9	15.2	1.52	3.43	1.97	0.01	47.73	2.44	0.55	0.61	0.23	BD	0.10	0.28	2.33	1.70	BD	3.24	0.86	1.44
	1.90	1.80	2.00	0.10	174	12.1	14.4	0.75	1.86	1.79	BD	25.71	1.33	0.62	0.49	0.24	BD	0.07	0.30	2.49	2.01	BD	1.68	0.86	1.55
	2.10	2.00	2.20	0.04	115	8.8	13.1	0.63	1.41	1.52	BD	15.07	0.82	0.76	0.62	0.26	BD	0.06	0.40	3.12	1.94	BD	1.33	1.07	1.96
	2.30	2.20	2.40	0.03	76	6.0	12.7	0.54	1.89	0.59	0.01	9.69	0.52	0.90	1.07	0.18	0.01	0.06	0.53	3.60	0.90	BD	1.48	1.44	2.33
	2.50	2.40	2.60	0.05	12	1.3	9.2	0.12	0.74	0.16	BD	0.98	0.41	0.94	0.08	0.01	0.02	0.36	3.08	0.32	BD	0.49	0.88	1.90	
	2.80	2.60		0.49	1.5	0.15	9.8	0.03	0.15	0.07	BD	0.00	BD	0.03	0.21	0.01	BD	BD	0.04	1.19	0.04	BD	0.11	0.14	0.63
	BULK				125	8.4	14.9	0.68	1.54	1.15	0.07	19.22	1.48	0.25	0.46	0.09	N.A.	N.A.	0.13	1.60	0.85	N.A.	1.45	0.48	0.93

N.A.: Not Available. BD: Below Detection.

- The metal extraction was not conducted for the lowest-density fraction of A-8 soil due to the very small recovery of this fraction. We thus assumed that the extractable element concentration in this fraction were the same as those in the A-9 soil which is adjacent to A-8 plot as a part of long-term field experiment in Yamanashi, Japan.

1080

1085

Table A2. The results of qubic polynomical regression model applied to each of the four soil groups for pyrophosphate-extractable organic C (DOC_{PP}) and the sum of pyrophosphate- and oxalate-extractable C ($DOC_{PP}+DOC_{OX}$).

	Allophanic Andisol	Non-allophanic Andisol	Spodic	Crystalline mineralogy
	DOC_{PP}			
r^2	0.17	0.41	0.55	0.50
RMSE	0.12	0.24	0.12	0.11
n	49	27	14	39
F	3.13	5.21	4.05	11.86
p	0.0347	0.0068	0.040	<0.0001
	$DOC_{PP}+DOC_{OX}$			
r^2	0.32	0.47	0.55	0.51
RMSE	0.12	0.22	0.12	0.11
n	49	27	14	39
F	6.99	6.73	4.12	12.27
p	0.0006	0.0020	0.0384	<0.0001

1090